

See discussions, stats, and author profiles for this publication at: <https://www.researchgate.net/publication/256763434>

Entangled Photon-Pair Two-Dimensional Fluorescence Spectroscopy (EPP-2DFS)

ARTICLE *in* THE JOURNAL OF PHYSICAL CHEMISTRY B · SEPTEMBER 2013

Impact Factor: 3.3 · DOI: 10.1021/jp405829n · Source: PubMed

CITATIONS

6

READS

112

4 AUTHORS:



[Michael Raymer](#)

University of Oregon

228 PUBLICATIONS 6,865 CITATIONS

[SEE PROFILE](#)



[Andrew H Marcus](#)

University of Oregon

81 PUBLICATIONS 1,404 CITATIONS

[SEE PROFILE](#)



[Julia R Widom](#)

University of Michigan

20 PUBLICATIONS 119 CITATIONS

[SEE PROFILE](#)



[Dashiell L. P. Vitullo](#)

University of Oregon

3 PUBLICATIONS 15 CITATIONS

[SEE PROFILE](#)

Entangled Photon-Pair Two-Dimensional Fluorescence Spectroscopy (EPP-2DFS)

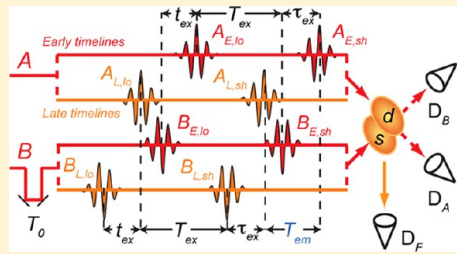
M. G. Raymer,^{*,†} Andrew H. Marcus,^{*,‡} Julia R. Widom,[‡] and Dashiell L. P. Vitullo[†]

[†]Oregon Center for Optics and Department of Physics, University of Oregon, Eugene, Oregon 97403, United States

[‡]Oregon Center for Optics, Institute of Molecular Biology and Department of Chemistry and Biochemistry, University of Oregon, Eugene, Oregon 97403, United States

Supporting Information

ABSTRACT: We introduce a new method, called entangled photon-pair two-dimensional fluorescence spectroscopy (EPP-2DFS), to sensitively probe the nonlinear electronic response of molecular systems. The method incorporates a separated two-photon ('Franson') interferometer, which generates time-frequency-entangled photon pairs, into the framework of a fluorescence-detected 2D optical spectroscopic experiment. The entangled photons are temporally shaped and phase-modulated in the interferometer, and are used to excite a two-photon-absorbing (TPA) sample, whose excited-state population is selectively detected by simultaneously monitoring the sample fluorescence and the exciting fields. In comparison to 'classical' 2DFS techniques, major advantages of this scheme are the suppression of uncorrelated background signals, the enhancement of simultaneous time-and-frequency resolution, the suppression of diagonal 2D spectral features, and the enhancement and narrowing of off-diagonal spectral cross-peaks that contain information about electronic couplings. These effects are a consequence of the pure-state field properties unique to a parametric down-conversion light source, which must be included in the quantum mechanical description of the composite field-molecule system. We numerically simulate the EPP-2DFS observable for the case of an electronically coupled molecular dimer. The EPP-2DFS spectrum is greatly simplified in comparison to its classical 2D counterpart. Our results indicate that EPP-2DFS can provide previously unattainable resolution to extract model Hamiltonian parameters from electronically coupled molecular dimers.



I. INTRODUCTION

In the past several years, major advances have been made in quantum chemistry (QC) and quantum information science (QIS), and these fields are now beginning to strongly impact one another.^{1–3} A long-standing goal of QC is to understand the interplay of excited electronic states and chemical reactivity. For example, chemical reactions that involve electronic charge or energy transfer between coupled molecular chromophores can be described in terms of molecular Hamiltonians, which take into account intermolecular state-to-state couplings, coherence time scales, and transition rates.^{4–6} At the same time, significant progress has been made in QIS to understand the physical nature of information, including the concept of quantum entanglement, which is viewed as a 'resource' for techniques such as quantum cryptography and quantum teleportation.^{7–9}

This work advances the question of what can be accomplished using quantum-entangled light in molecular spectroscopy that is not otherwise possible using standard ('classical') approaches. 'Classical' light may be described as an ideal monochromatic coherent state, or as a statistical mixture of such states.¹⁰ 'Quantum' or 'nonclassical' light, on the other hand, can exhibit time-frequency entanglement and interference at the quantum-phase level, and must be described in terms of quantum-state wave functions. A number of theoretical

proposals and experiments have addressed this question in the context of time-frequency entangled light (see section II below). Although such studies establish the plausibility of using nonclassical light to outperform conventional spectroscopic measurements, new information about molecular structure and dynamics are yet to emerge from these ideas.

Here we propose a new nonlinear spectroscopic scheme, which we call entangled photon-pair two-dimensional fluorescence spectroscopy (EPP-2DFS). Our approach combines two central techniques of QIS and QC: the separated two-photon ('Franson') interferometer,^{11–13} and the method of fluorescence-detected ultrafast two-dimensional (2D) optical coherence spectroscopy.^{14–18} Unlike conventional 2D optical coherence methods,^{19,20} EPP-2DFS uses a continuous-wave (cw) source of time-frequency entangled photon pairs to excite a two-photon absorbing molecular system. Detection of the ensuing weak fluorescence, while simultaneously monitoring the exciting fields, allows us to achieve simultaneous high time and frequency resolution, which is not possible using any

Special Issue: Michael D. Fayer Festschrift

Received: June 14, 2013

Revised: August 6, 2013

classical light source. The proposed scheme is also significantly different from other recent proposals to use entangled photon pairs for 2D spectroscopy,^{21–23} as explained below.

In QIS and quantum optics, a central concept is that of the ‘detector.’ Without well-behaved detectors, there could be no tests of quantum entanglement or local realism via violations of Bell’s inequality, and no tests of the quantum theory of light. A large body of research in quantum optics details the ways in which detectors interact with light to provide information about the state of that light. In QC, these roles are reversed. Light from a ‘classical’ source, such as a laser, is used to obtain information about the molecules. When viewed in more detail, both the light and the molecules are quantum objects, with the molecules acting as detectors. In order to understand this interaction completely, one must treat both types of objects quantum mechanically. By analyzing a prototypical experiment in quantum optics, we show how such experiments can be modified to provide information about the detectors (or in our case, molecules acting as detectors) as revealed by the quantum nature of light.

A unique signature of using two-photon nonclassical light for spectroscopy was predicted^{24,25} and demonstrated in early experiments by Georgiades, et al., who showed that in atomic cesium, a two-photon absorption (TPA) process with a resonant intermediate state occurs at a rate that is linearly proportional to the light flux, rather than the quadratic dependence observed with classical light.^{26,27} This occurs because, in perfectly number-correlated light beams, the flux of photon pairs is linearly proportional to the flux of single photons. This same effect was observed for TPA in a porphyrin dendrimer, in which case the intermediate states were nonresonant.²⁸ Several theoretical studies have proposed to use two-photon nonclassical light to perform ‘virtual-state spectroscopy,’ which in principle can probe the structure of unpopulated intermediate states,^{29–32} although such studies have not been realized experimentally. Experiments have shown the capability of time-frequency entangled light to resolve a two-photon resonance with high spectral resolution, and to simultaneously probe the two-photon molecular response on ultrafast time scales.^{33,34} This feature of light from two-photon sources is exploited in the present work. Such experiments have been applied and extended to TPA in organic thiophene dendrimers.³⁵ Additional theoretical analyses have been carried out to explore the properties of time-frequency entangled light in spectroscopy, including general^{36,37} and specific studies of molecular vibronic states³⁸ and semiconductor quantum wells.^{21,31}

2D optical spectroscopy is a nonlinear technique in which molecules are excited using a sequence of coherent laser pulses that are variably delayed in time, and the resulting measured signals are Fourier-transformed from the time-delay variables to their corresponding frequency variables.^{19,20} An important advantage of the 2D spectroscopic approach, in comparison to linear spectroscopy, is that it allows the cross couplings between energy eigen-states to be determined. Roslyak and Mukamel introduced the concept of 2D optical spectroscopy using time-frequency entangled light sources.²² In their approach, one of the interpulse time delays present in classical 2D spectroscopy is replaced by a variable entanglement time, which is a parameter in the description of the two-photon entangled state.²² Richter and Mukamel subsequently proposed a variant of this technique that uses four distinct light beams

containing a total of four photons (two distinct entangled photon pairs).²¹

Our proposed arrangement is distinct from prior schemes in that we employ a single entangled photon pair that is divided into two beams, which experience unequal transit times on their way to the sample. This is accomplished by using a separated two-photon interferometer (herein referred to as a Franson interferometer)^{11–13} as the excitation source for a two-dimensional fluorescence spectroscopy (2DFS) experiment.^{14–18} In 2DFS, the phase of the delayed optical fields are rapidly modulated (and simultaneously monitored), and the nonlinear fluorescence signal is phase-synchronously detected. The high sensitivity afforded by the 2DFS technique is especially useful in this context, since entangled photon-pair experiments must be carried out in the low-signal, photon-counting regime.

In EPP-2DFS, we incorporate the Franson interferometer into a standard 2DFS experimental setup. Time-frequency entangled photon-pairs are generated by parametric down-conversion (PDC) at the source nonlinear optical crystal, which is pumped using a spectrally narrow cw laser. The entangled photon-pairs are directed through the Franson interferometer with variable phases and delays in both emitted light paths. The entangled photon pair is used to excite a TPA sample, and the ensuing fluorescence is detected while simultaneously monitoring the phase and signal of the exciting field. These signals are measured as the delays are systematically varied, and the resulting nonlinear response is Fourier transformed to obtain 2D spectra. Our calculations indicate that this setup will operate in highly useful ways in comparison to standard 2D electronic spectroscopies, which use classical laser pulses as probes. In particular, (1) the intensities of nonlinear optical signals will be greatly enhanced relative to those of linear ‘background’ signals, resulting in (nonlinear) signal-to-(linear) background ratios much greater than unity. In experiments that use conventional light sources, this ratio is normally much less than unity. (2) The time-frequency entanglement present in the light source allows simultaneous temporal and spectral resolution that is not possible using any ‘classical’ light source, such as short laser pulses or broadband thermal-like light. (3) The 2D spectral line shapes of resonant transitions will be much narrower than for experiments that use conventional light sources. The 2D line widths will be proportional to the inverse excited state population relaxation time scale, rather than the dephasing time scale, thus providing considerable enhancements to spectral resolution. Furthermore, the proposed approach can be used to isolate the TPA signals that contribute primarily to the cross-peaks of 2D optical spectra. This makes EPP-2DFS a potentially useful technique to elucidate the conformation of exciton-coupled molecular dimers. While points 1 and 2) can be considered extensions of previously known properties of entangled light spectroscopy,^{24,25,28,29,33–35,39} point 3 is an entirely new result unique to our specific experimental arrangement.

II. THE FRANSON SEPARATED TWO-PHOTON INTERFEROMETER

An intriguing experimental apparatus for studying the quantum nature of entangled photon-pairs is the separated two-photon interferometer, named after its inventor, James Franson.^{11–13} The Franson interferometer demonstrates a nonlocal quantum interference effect that cannot be simulated fully using a classical wave model for light. As shown schematically in Figure

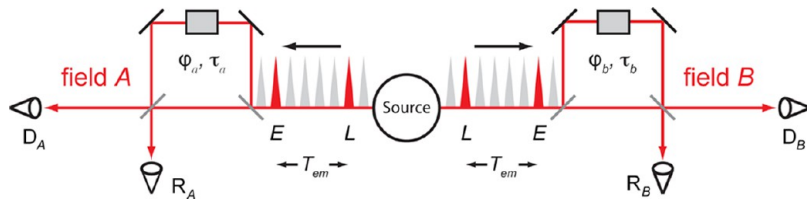


Figure 1. Franson interferometer. A stationary source creates two fields A and B , each of which enters an interferometer that introduces a relative time delay (τ_a, τ_b) in the long path. Phases (φ_a, φ_b) are controlled using acousto-optic Bragg cells (shown as gray rectangles). Gray diagonal lines are 50/50 beam splitters. Detectors D_A , D_B , R_A , and R_B generate photoelectric counts, and both coincident and individual detector count rates are recorded, yielding both phase (eq 2) and flux (eq 1) information, respectively. The source emission-time difference, denoted by T_{em} , is defined as the time between an ‘early’ (E) occurrence of the photon-pair virtual emission event in the source, and a ‘late’ (L) virtual emission event.

1, two spectrally correlated fields from a two-photon source (typically a PDC crystal) enter separate interferometers (labeled A and B). Each interferometer has one arm delayed by a time (τ_a and τ_b) that is much greater than the coherence time of the light to prevent one-photon interference, as is typically seen in ordinary interferometers. The relative path delays of the A and B interferometers are set equal to within the coherence time of the light.⁴⁰ The average detection rate (i.e., the light intensity or photoelectron count rate) at detectors D_A and D_B is independent of any subwavelength phase shifts (φ_a, φ_b) in the interferometer arms. Nevertheless, the rate of coincident detection at D_A and D_B is found to depend on the phase shifts in either interferometer, which is a nontrivial consequence of photon correlation. While this effect can be partially simulated using a classical wave model, experimental observations allow for a clear distinction to be made between quantum and classical behavior. For certain two-photon states of the fields, quantum theory predicts 100% fringe visibility, whereas classical theory predicts visibility no greater than 50%.¹²

Franson described this result in terms of “a quantum-mechanical field corresponding to an entangled pair of coincident photons, with a superposition of times at which the pair may have been emitted.”¹² We refer to this effect as ‘emission-time freedom,’ and we regard the possible emission events as ‘virtual.’ Each emission event can occur over a range of indeterminate times. During the period between the first interaction and the final interaction, the combined field-detector system is in a state where the energy in the field alone is indeterminate, as is the energy of the detector alone, while the total energy in the joint system is determinate. Therefore, in analogy to a virtual photon being exchanged between two electrons in a scattering event, we say the emission events are not ‘real,’ but ‘virtual.’

We illustrate this concept schematically in Figure 1 by the sequence of many potentially emitted virtual wave packets on each side of the source. None of the packets should be viewed as photons actually emitted, but as quantum amplitudes for possible emission of a correlated pair at a certain time. The sequence of packets shown represents a single pair of photons being emitted, but with emission-time freedom for the pair.

Two-photon interference occurs because two indistinguishable ‘paths’ can realize a coincidence outcome. For example, a pair of photons could be emitted at a certain time (labeled E for early), and arrive at the detectors by traversing the long paths in the interferometers. Alternatively, a pair could be emitted at a later time (labeled L for late) that is delayed by exactly the difference between the long and short path propagation times, and arrive at the detectors by traversing the short paths. Because these processes (or paths) leading to the same

outcome are physically indistinguishable when the delays are identical to within the two-photon coherence time, their quantum probability amplitudes add coherently and create quantum interference. Franson showed that for certain combinations of the interferometer phases, the probability for a coincidence at detectors D_A and D_B is zero, as a result of destructive interference between the two paths leading to this outcome. We next attempt to model this effect using classical fields, in the spirit of refs 12 and 41, and then review the full quantum treatment.

A. Classical Theory of the Franson Interferometer. We consider the classical field amplitudes A and B , with respective phases $\phi(t)$ and $\sigma\phi(t)$, which rapidly and randomly fluctuate. We write the fields as $Ae^{i\phi(t)}$ and $Be^{i\sigma\phi(t)}$, respectively. Because the time derivative of $\phi(t)$ is the instantaneous frequency, the fluctuating phase gives the fields broad bandwidth, where $\sigma = \pm 1$ indicates whether the fields are frequency correlated (+1) or anticorrelated (-1). For the case of frequency-correlated fields, the frequencies fluctuate concertedly, while for anticorrelated fields, the frequency fluctuations cancel so that their sum is a constant at all times. The carrier frequencies ω_A and ω_B of fields A and B , respectively, may be either equal, or unequal, to each other. Assuming statistically stationary fields, the average numbers of photoelectron counts at detectors D_A and D_B during a short integration time window T_w are

$$N_A = \eta T_w \frac{A^2}{2\hbar\omega_A}, \quad N_B = \eta T_w \frac{B^2}{2\hbar\omega_B} \quad (1)$$

where η is the detector quantum efficiency, and the factors $A^2/2$ and $B^2/2$ are the average beam power expressed in watts. Interference terms are absent from eq 1 because the interferometer delays exceed the field’s coherence time. While the light is in the long arm, the frequency of the light at the interferometer input rapidly fluctuates across the broad spectral bandwidth of the field, thus destroying any interference at the detectors.

The average number of coincidence counts at detectors D_A and D_B within a short integration time window T_w is

$$N_{AB} = N_A N_B \frac{1}{2} [2 + \cos(\varphi_a - \sigma\varphi_b)] \quad (2)$$

This interference shows a 50% fringe visibility, which is the greatest possible using classical wave theory, regardless of the model used.^{12,41} Equation 2 shows that in this classical model, the phase signatures $\cos(\varphi_a - \varphi_b)$ and $\cos(\varphi_a + \varphi_b)$ act as identifiers for frequency correlation and anticorrelation, respectively.

B. Quantum Mechanical Treatment of Two-Photon Interference. Unlike the classical result described by eq 2, a

quantum mechanical treatment of a two-photon state created in a Franson interferometer predicts an interference visibility up to 100%.^{11,12,40} This difference between quantum and classical behaviors arises from a distinction between the interference of classical electromagnetic fields and the interference of quantum mechanical probability amplitudes. If the light source is a nonlinear optical crystal pumped by a high-frequency cw laser beam, photon-pairs are created by PDC.^{10,42} The photons of each pair are frequency anticorrelated and temporally correlated; that is, they are temporally-spectrally entangled.¹¹ The paired photons travel from the source in opposite directions and encounter the separate interferometers. The difference between the times of flight through the long and short paths is much greater than the duration of a single-photon wave packet, which is equal to the inverse of the light's spectral bandwidth. Because the short-path and long-path portions of each photon wave packet do not overlap in time, they do not interfere, and consequently the counting rate at each detector does not change when either of the phases is varied. The numbers of photoelectron counts in a short integration time window T_w , averaged over many trials, are

$$N_A = \frac{\eta T_w}{2} \langle A^\dagger(t)A(t) \rangle \quad \text{and} \quad N_B = \frac{\eta T_w}{2} \langle B^\dagger(t)B(t) \rangle \quad (3)$$

where $A(t)$ and $B(t)$ are photon annihilation operators for each beam emerging from the source. We define the photon flux in each beam from the source Φ as the mean number of photon pairs generated per second. The average numbers of photoelectron counts in a short time window T_w are

$$N_A = N_B = \frac{\eta T_w}{2} \Phi \quad (4)$$

We note that the factor of 1/2 appears in eq 4 because half of the photons exit the 'reference' ports, labeled R_A and R_B in Figure 1.

The average number of coincidence counts at the detectors D_A and D_B within a short integration time window T_w is given by¹¹

$$N_{AB} = T_w \eta^2 \frac{\Phi}{8} [1 + \cos(\varphi_a + \varphi_b)] \quad (5)$$

This result holds when the time delays in the interferometers are much longer than the coherence time of the light, and set equal to a precision within the coherence time of the light (i.e., the inverse spectral width).⁴⁰ We note for completeness that the coincidence rate between detectors R_A and R_B is also given by eq 5, while the coincidence rate between R_A and D_B , or between D_A and R_B , is given by eq 5 with \cos replaced by $-\cos$. We note that the term $\cos(\varphi_a + \varphi_b)$ is consistent with the classical result for frequency anticorrelation. Moreover, the interference visibility is seen to equal 100%, in contrast to the classical result. This can be understood in terms of the Feynman formulation of quantum mechanics. There are two different, but indistinguishable, paths in state space that can lead to the same final state. For certain quantum phase combinations, these pathways interfere destructively, leading to a zero coincidence-count rate. At these phase combinations, all coincidence counts are between either the pair D_A and D_B , or the pair R_A and R_B , but there are no coincidences between one D and one R detector. The interference leading to this result is quantum amplitude interference, not electromagnetic field interference. With classical electromagnetic field phase

interference, the visibility could be 50% at most, due to the absence of quantum entanglement in the classical theory. As we discuss further below, the effect of two-photon quantum entanglement leads to the novel capability for simultaneous time-and-frequency resolution, in contrast to the classical-field case.

Another important observation is that the coincidence-count rate, described by eq 5, is proportional to the photon flux Φ in a single beam, rather than the product of the two beam fluxes. Hence, the two-photon coincidence rate scales linearly with the beam intensities, unlike the quadratic scaling that would occur in the classical case. The linear scaling is due to the perfect number correlation between the two beams: for each count at detector D_A , there is guaranteed to be a count either at detector D_B or at reference port R_B , but these counts are not necessarily coincident. This effect is central for experimental applications to molecular spectroscopy, as was pointed out in a different context.²⁸

The characteristic properties of the separated two-photon interferometer, predicted by Franson, were experimentally verified.^{13,41,43} These effects constitute an illustration of the absence of local realism in situations that are uniquely described by quantum mechanics. In this sense, they are similar to violations of the Bell inequalities.¹¹

It is useful at this point to consider why typical experiments in quantum optics provide information about the light that is detected, but not about the properties of the detectors. We note that the oscillation in the coincidence count rate of the two-photon interferometer depends only on the quantum state of the light and on the settings of the interferometers, but not on any properties of the detectors. The theory used by Franson to predict the experimental outcome treats the detectors as having infinite spectral bandwidth and instantaneous response. In this idealized limit, it is unnecessary to consider the quantum state of the detectors since no quantum memory effects are possible. Even though the detectors in the two-photon interferometer are macroscopic objects, which presumably obey classical physics, their final state outcome is determined by quantum interference between different Feynman paths of the photon-pair. This observation provides a link between quantum optics and nonlinear molecular spectroscopy. In 2D optical spectroscopy, for example, the observed signals can be attributed to following different Feynman pathways through the quantum Liouville space.¹⁹ By replacing the classical detectors in the two-photon interferometer with molecules, we may follow this line of reasoning into the quantum-detector regime.

III. COUPLED TWO-LEVEL MOLECULES AS A QUANTUM TWO-PHOTON COINCIDENCE DETECTOR

In Figure 2a, we illustrate an experimental arrangement that uses the fields A and B from the Franson interferometer to resonantly excite a pair of electronically coupled two-level molecules. Standard photon-counting detectors are placed at positions just after the sample to determine whether zero, one or two photons have been absorbed by the molecules. Fluorescence is also detected from the sample.

The fields A and B that emerge from the Franson interferometer exhibit a constant average flux. They consist of sparsely distributed single-photon wave packets that possess (ideally) perfect number correlation in time between fields A and B . The duration of each packet can be in the femtosecond

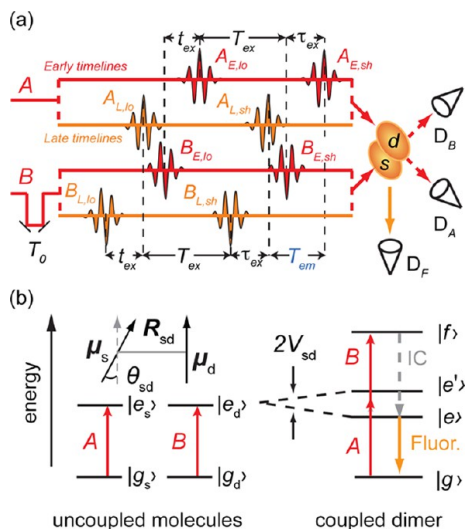


Figure 2. (a) Beam excitation and optical detection geometry for entangled pulse-pair 2D fluorescence spectroscopy (EPP-2DFS) performed on a pair of electronically coupled molecules, which are labeled *s* and *d*. A variable delay T_0 is included in the *B* beam. Single-photon wave-packets are shown as short oscillatory pulses, with perfect number correlation between fields *A* and *B*. Leading packets in each field correspond to those that traversed the short interferometer paths, while the lagging packets traversed the long paths. Both ‘early’ and ‘late’ timelines are shown, which correspond to virtual emission events separated by the variable emission time interval T_{em} . (b) Energy-level diagram of a pair of uncoupled two-level molecules (left), and that of a coupled molecular dimer (right). TPA results in population on the doubly excited $|f\rangle$ state, followed by internal conversion (IC) and fluorescence from the lowest energy singly excited $|e\rangle$ state.

regime, depending on the bandwidth of the fields. Even though the fields are stationary, when used to perform molecular spectroscopy, it is possible to monitor molecular dynamics on femtosecond time scales. This is similar in spirit to earlier studies of ‘fluctuation spectroscopy,’ which used built-in correlations between classical random broadband fields to extract ultrafast dynamics from atoms and molecules.^{44–46} Nevertheless, those fluctuation spectroscopic techniques are necessarily limited in their simultaneous time-and-frequency resolution, as explained in section IV below.

In each PDC event in the source (the actual time of which is indeterminate in the quantum sense), a single pair of femtosecond-duration photons is created, and after passing through the Franson interferometer, the photon pair is directed through the sample. The photon-packet amplitudes are shown as oscillatory pulses in Figure 2a. By choosing the path lengths within each of the interferometer arms, and adding an additional delay T_0 into the *B* beam, we can construct a four-pulse sequence of impinging photon wave packets, analogous to the four-pulse sequences typically used in classical 2DFS.^{14–17} Nevertheless, even though there are four ‘pulses’ created by each PDC event, there are only two photons. As we discuss further below, this is a useful feature of EPP-2DFS.

The TPA molecular response will be largest when interactions with the *A* and *B* photons occur nearly simultaneously, within a time window set by the relaxation time scales of intermediate molecular states. As previously described for the Franson interferometer (using standard photodetectors), there are two ways this can occur. In the first case, the photon pair is emitted ‘early,’ and both take their

respective long paths. Alternatively, the pair is emitted ‘late,’ and both take their respective short paths. The amplitudes for these two processes can interfere if the difference between the interferometer delays is not much greater than the relevant relaxation times of the molecule. This situation is different from the Franson (standard detector) case, for which the interference occurs only if the difference between the interferometer delays is not much greater than the coherence time (inverse bandwidth) of the light. The standard detector acts incoherently, with an infinitely rapid response and dephasing rate. If molecules replace the detectors, there is a coherent response interval that may be much longer than the coherence time of the light, during which the photon amplitude packets can arrive separately and interfere coherently. The molecules function as a ‘coherent signal integrator.’

In Figure 2b, we show the energy-level diagrams of a pair of two-level molecules, labeled *s* and *d*, which can experience a variable coupling V_{sd} . In the point-dipole approximation, the sign and magnitude of the coupling depends on the relative separation R_{sd} and orientation θ_{sd} of the molecular transition dipole moments μ_s and μ_d .^{15–18,47} The effect of nonzero coupling is to mix molecular states, so that excitations are delocalized between the two molecules. This coupling breaks the degeneracy of the one-exciton (or singly excited) states, labeled $|e\rangle$ and $|e'\rangle$. The ground state $|g\rangle$ is the zero-exciton state, and the biexciton (or doubly excited) state is labeled $|f\rangle$. The two incident photons *A* and *B* have femtosecond durations, and may or may not be close to resonance with the one-exciton transitions. The coupling determines the energy level spacings and the strengths of the collective transition dipole moments, which can be adjusted by varying the angle and separation between the molecules.⁴⁷

We consider the final-state outcomes from a molecular dimer that is excited by an entangled photon pair. For the case of zero coupling, each molecule may absorb a photon, and each in turn may give rise to an independent photoelectron count at the fluorescence detector. However, when the coupling is nonzero, the excited electronic states are delocalized between the two molecular sites. The coupled dimer can therefore undergo TPA to produce population on the doubly excited $|f\rangle$ state that can subsequently undergo internal conversion (IC) to the lowest energy singly excited $|e\rangle$ state, which in turn emits a single fluorescent photon. Detection of a fluorescent photon at D_F that is coincident with zero detected signals at D_A and D_B indicates that the coupled molecular dimer may have absorbed both photons, thus producing population on the $|f\rangle$ state. When using classical light fields, there are three possible quantum Liouville pathways that can produce population on the $|f\rangle$ state. These are illustrated in Figure 3, and are termed the TPA double-quantum coherence (DQC), rephasing (RP), and nonrephasing (NRP) pathways.^{16,19,20} Separation of these terms from ‘background’ signals, which arise independently from one-photon transitions of separated molecules, can be accomplished by phase-synchronous detection of the fluorescence, as is commonly practiced using classical 2DFS.^{14,16,17}

It is important to point out that the nonlinear optical response arising from a coupled two-level system (depicted in Figure 2b), which is most often measured using ‘classical’ four-wave-mixing (FWM) approaches to 2D coherence spectroscopy (2DCS), is nonzero only for Liouville pathways in which transitions between the ground and singly excited states do not exactly cancel (i.e., destructively interfere) with transitions between singly excited and doubly excited states. This issue has

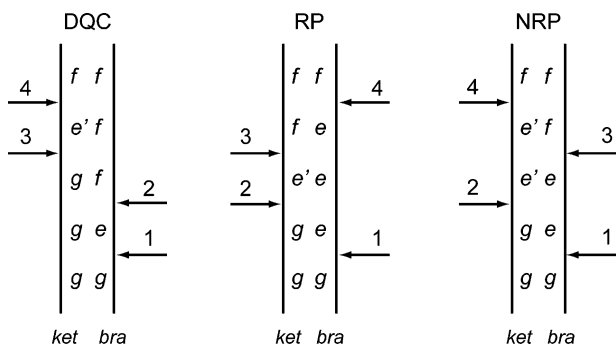


Figure 3. Double-sided Feynman diagrams for the molecular density matrix corresponding to the three possible TPA excitation pathways that produce population on the $|f\rangle$ state of an electronically coupled molecular dimer. The three different pathways are designated double-quantum coherence (DQC), rephasing (RP), and nonrephasing (NRP). Time increases in the upward direction. Horizontal arrows indicate field-molecule interactions, which induce transitions between populations and coherences during the time-evolution of the density operator. Arrows appearing on the left indicate an interaction on the ket side of the density matrix, while arrows appearing on the right indicate a bra-side interaction.

recently been discussed in the context of 2DCS experiments performed on a dilute atomic vapor by Dai et al.⁴⁸ Thus, in order to generate a FWM signal, some asymmetry is required in the coupled system, either in the form of a binding energy to break the degeneracy between the $|e\rangle,|e'\rangle \leftarrow |g\rangle$ and $|f\rangle \leftarrow |e\rangle,|e'\rangle$ transitions, or the manifestation of different oscillator strengths bridging these transitions. The situation is different for ‘classical’ 2DFS experiments, in which the IC process (or self-quenching) of the doubly excited state serves to break the cancellation that would otherwise occur between signal contributions involving $|e\rangle,|e'\rangle \leftarrow |g\rangle$ transitions and those involving $|f\rangle \leftarrow |e\rangle,|e'\rangle$ transitions.¹⁶ Thus, for ‘classical’ 2DFS experiments, no additional anharmonicity is required to produce a nonlinear optical response from the coupled molecular dimer. The situation is even more complex for EPP-2DFS experiments. It is known that the mere presence of frequency anticorrelation in the A and B driving fields is sufficient to create a resonant TPA response for two independent (uncoupled) molecules when the sum of the two field frequencies $\omega_p = \omega_A + \omega_B$ is slowly swept through the sum of the two molecules’ separate resonance frequencies $\omega_0 = \omega_s + \omega_d$.^{49,50} We consider this process in the SI section, where we show that EPP-2DFS signals resulting from the TPA of a coupled molecular dimer will depend on the $\cos(\varphi_a + \varphi_b)$ phase signature, while ‘background’ signals arising from the correlated one photon absorption of A and B photons by distant molecules will depend on either the phase of the A beam or that of the B beam alone.

IV. TIME-FREQUENCY PHOTON ENTANGLEMENT: AVOIDING THE TIME-FREQUENCY UNCERTAINTY PRINCIPLE

We emphasize that the photon pairs created by the stationary PDC process are spectrally entangled. In the present case, this corresponds to a two-photon field state in which the frequency of each photon is indeterminate in the quantum sense, but it is guaranteed that the sum of their frequencies is fixed to a known value.^{10,39} Thus, measuring the frequency of one photon completely determines the frequency of the other, in spite of

the fact that both were previously indeterminate. In addition, the two photons are tightly correlated in time (for example, to within 10 fs), so that measuring the arrival time of one guarantees the arrival time of the other. There is no theoretical limit to the simultaneous tightness of both spectral and temporal correlation, as might be expected from a naïve application of the Heisenberg Uncertainty Principle.^{51,52} We show here that only nonclassical fields can circumvent this limit.

The A and B fields are broadband, possibly with femtosecond coherence times, and with center frequencies ω_A and ω_B , respectively. However, because the field pumping the PDC is assumed to be monochromatic, the instantaneous frequencies of A and B photons (ω and ω' , respectively), if measured, are found to be perfectly anticorrelated so that they add to the pump frequency: $\omega + \omega' = \omega_p$. If instead the arrival times (t and t') of the photons are measured, it is found that they are perfectly correlated, i.e., that $t = t'$. Thus, for a quantum two-photon field, there is no lower bound on the uncertainty product $\text{std}(\omega + \omega')\text{std}(t - t')$, where std stands for standard deviation. This is analogous to the famous EPR state of two quantum particles, where the uncertainty product $\text{std}(x + x')\text{std}(p - p')$ for position x and momentum p has no lower bound, indicating quantum entanglement, which cannot be mimicked by any classical model (particle or wave). This property affords the possibility to achieve simultaneous high temporal and spectral resolution.^{33,34}

To verify that only nonclassical fields can exhibit the properties described above, we consider how small the uncertainty product can be for the case of two classical light pulses, irrespective of their degree of correlation. This can be addressed using the same mathematics as applied to verify the absence of entanglement for the case of (generalized) position and momentum variables.^{51,52} For all separable (nonentangled) states, which automatically includes all classical ones, this leads to the lower bound

$$\text{std}(\omega + \omega')\text{std}(t - t') \geq 1 \quad (6)$$

where the equality holds when the two pulses have identical temporal durations and are transform limited. We note that the uncertainty product defined in eq 6 is twice as large as the familiar bound for the time-frequency uncertainty product for a single classical pulse, i.e., $\text{std}(\omega_i)\text{std}(t_i) \geq 1/2$. Furthermore, the presence of classical correlations between the A and B fields, as occurs in ‘fluctuation spectroscopy’,^{44–46} can only make the uncertainty product larger. Thus, this is not the optimal classical scheme for achieving simultaneous time and frequency resolution. The best possible solution to minimize the uncertainty product with classical pulses (i.e., pulses created by a laser or other conventional sources) is by using two transform-limited pulses of identical durations, and with possibly different carrier frequencies. This places a strict limit on how well classical light pulses can achieve simultaneous time and frequency resolution, which does not apply to quantum fields because they can admit entanglement.

The usefulness of this type of time-frequency entanglement is in exciting a specific set of molecules that have a common two-photon resonance frequency, while also having tight coincidence between the interaction times of the two photons with the molecule.^{33,34} The former allows the selection of a homogeneously broadened subgroup of molecules from within a broader inhomogeneous distribution. The latter means that molecules with a very short lifetime of the intermediate state in the two-photon transition can still be efficiently excited. These

two conditions cannot be met simultaneously using any classical light source.

V. TWO-DIMENSIONAL FLUORESCENCE SPECTROSCOPY USING ENTANGLED PHOTON PAIRS

We use a particular experimental delay order in which all delays (τ_a , τ_b , T_0 in Figures 1 and 2) are positive and interrelated, such that a single source emission event at time zero creates four possible interaction times, which obey the time ordering $0 < T_0 < \tau_a < (T_0 + \tau_b)$. The virtual emission event at time zero is illustrated at the top of Figure 4, and labeled ‘early emission

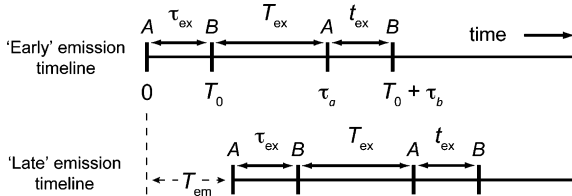


Figure 4. Top timeline: An early virtual emission event in the source creates a sequence of four possible interaction times with the molecule, with delays fixed by the experimental configuration. Bottom timeline: A later virtual emission event in the source, delayed by an indeterminate time T_{em} , creates another sequence of four possible interaction times with the molecule.

timeline.’ The experimentally controlled intervals between these times are denoted $\tau_{\text{ex}} \equiv T_0$, $T_{\text{ex}} \equiv \tau_a - T_0$, and $t_{\text{ex}} \equiv T_0 + \tau_b - \tau_a$. The possible interaction times are labeled in the order ABAB because the B field has been additionally delayed by the time T_0 , causing it to arrive at the sample after the A field (see Figure 2a). Given that virtual emission events can occur at any time, and that multiple emission times contribute to the Feynman diagrams for the processes being considered, we also illustrate in Figure 4 a second ‘late emission timeline,’ which is due to a virtual emission that is delayed from the first by an indeterminate time T_{em} . This effect creates four additional possible times of interaction with the molecule: $T_{\text{em}} < (T_{\text{em}} + T_0) < (T_{\text{em}} + \tau_a) < (T_{\text{em}} + T_0 + \tau_b)$. For the case of two-photon excitation considered here, exactly two virtual emission events need to be considered, so that four of eight potential interaction times may contribute to a given Feynman diagram. For example, it is allowed that for some diagrams, the earliest interaction will be with a B photon at time T_0 , with some combination of two A interactions and one additional B interaction at later times. We emphasize that even though there are four interactions in a given Feynman diagram, only two photons are involved. Hereafter we will use the intervals τ_{ex} , T_{ex} , and t_{ex} rather than the intervals T_0 , τ_a , and τ_b .

The theory for the nonlinear optical response of molecules using entangled photon pairs is based on the quantum perturbation theory that is used to analyze most experiments in ultrafast 2D spectroscopy [see the Supporting Information (SI) section for details of the derivation].^{19,20} In the current application, we generalize the theory to describe the evolution of the composite light-molecule density operator in the interaction picture, similar to the approach taken by other workers.^{21–23} The interaction Hamiltonian is the electric dipole interaction, $\hat{d}(t) \cdot \hat{E}(t)$, where the electric field at the location of the molecule is represented by the operator $\hat{E}(t)$, consisting of creation and annihilation operators for photons at particular frequencies. The initial state of the combined system has the

molecule in its ground state, $|g\rangle$, and the optical field in a two-photon spectrally entangled state $|\Psi\rangle_F$, as described above. We consider broadband light from a PDC source that is pumped by a cw monochromatic field of frequency ω_p , so that the frequencies of two emitted photons must sum to this value. The final state of interest is $|f\rangle|vac\rangle$, in which the molecule is in its doubly excited state $|f\rangle$, and the field is in the vacuum state (both incident photons have been absorbed). In fourth-order perturbation theory, the population of this final state created within a time window $[-\tau_w, \tau_w]$ is proportional to a weighted sum of three terms,

$$\begin{aligned} R_{\text{DQC}}^{e,e'} &= \int_{-\tau_w}^{\tau_w} dt_4 \int_{-\infty}^{t_4} dt_3 \int_{-\infty}^{t_3} dt_2 \\ &\quad \int_{-\infty}^{t_2} dt_1 e^{-\gamma_{eg}(t_2-t_1)} e^{-\gamma_{fg}(t_3-t_2)} e^{-\gamma_{fe}(t_4-t_3)} \\ &\quad \cdot \langle vac | \hat{E}^{(+)}(t_4) \hat{E}^{(+)}(t_3) | \Psi \rangle_{FF} \langle \Psi | \hat{E}^{(-)}(t_1) \\ &\quad \hat{E}^{(-)}(t_2) | vac \rangle \\ R_{\text{RP}}^{e,e'} &= \int_{-\tau_w}^{\tau_w} dt_4 \int_{-\infty}^{t_4} dt_3 \int_{-\infty}^{t_3} dt_2 \\ &\quad \int_{-\infty}^{t_2} dt_1 e^{-\gamma_{eg}(t_2-t_1)} e^{-\gamma_{ee}(t_3-t_2)} e^{-\gamma_{fe}^*(t_4-t_3)} \\ &\quad \cdot \langle vac | \hat{E}^{(+)}(t_3) \hat{E}^{(+)}(t_2) | \Psi \rangle_{FF} \langle \Psi | \hat{E}^{(-)}(t_1) \\ &\quad \hat{E}^{(-)}(t_4) | vac \rangle \\ R_{\text{NRP}}^{e,e'} &= \int_{-\tau_w}^{\tau_w} dt_4 \int_{-\infty}^{t_4} dt_3 \int_{-\infty}^{t_3} dt_2 \\ &\quad \int_{-\infty}^{t_2} dt_1 e^{-\gamma_{eg}(t_2-t_1)} e^{-\gamma_{ee}(t_3-t_2)} e^{-\gamma_{fe}(t_4-t_3)} \\ &\quad \cdot \langle vac | \hat{E}^{(+)}(t_4) \hat{E}^{(+)}(t_2) | \Psi \rangle_{FF} \langle \Psi | \hat{E}^{(-)}(t_1) \\ &\quad \hat{E}^{(-)}(t_3) | vac \rangle \end{aligned} \quad (7)$$

where the e, e' superscript indicates which combination of intermediate states a particular pathway goes through. We have adopted the standard terminology,^{16,19,20} where DQC stands for ‘double quantum coherence,’ RP stands for ‘rephasing,’ and NRP stands for ‘nonrephasing.’ The exponential damping functions in eq 7 are equal to the e, e' component of the appropriate molecular response functions

$$\begin{aligned} \langle f | \hat{\mu}^{(-)}(t_4) \hat{\mu}^{(-)}(t_3) | g \rangle \langle g | \hat{\mu}^{(+)}(t_1) \hat{\mu}^{(+)}(t_2) | f \rangle^{e,e'} \\ = [\mu_{eg} \mu_{fe} \mu_{ge} \mu_{e'f'}] e^{-\gamma_{eg}(t_2-t_1)} e^{-\gamma_{fg}(t_3-t_2)} e^{-\gamma_{fe}(t_4-t_3)} \\ \langle f | \hat{\mu}^{(-)}(t_3) \hat{\mu}^{(-)}(t_2) | g \rangle \langle g | \hat{\mu}^{(+)}(t_1) \hat{\mu}^{(+)}(t_4) | f \rangle^{e,e'} \\ = [\mu_{eg} \mu_{fe} \mu_{ge} \mu_{e'f'}] e^{-\gamma_{eg}(t_2-t_1)} e^{-\gamma_{ee}(t_3-t_2)} e^{-\gamma_{fe}^*(t_4-t_3)} \\ \langle f | \hat{\mu}^{(-)}(t_4) \hat{\mu}^{(-)}(t_2) | g \rangle \langle g | \hat{\mu}^{(+)}(t_1) \hat{\mu}^{(+)}(t_3) | f \rangle^{e,e'} \\ = [\mu_{eg} \mu_{fe} \mu_{ge} \mu_{e'f'}] e^{-\gamma_{eg}(t_2-t_1)} e^{-\gamma_{ee}(t_3-t_2)} e^{-\gamma_{fe}(t_4-t_3)} \end{aligned} \quad (8)$$

where $\gamma_{nm} = \tilde{\gamma}_{nm} - i\omega_{nm}$, $\gamma_{nm}^* = \tilde{\gamma}_{nm} + i\omega_{nm}$; $\omega_{nm} = \epsilon_{nm}/\hbar$, and $\tilde{\gamma}_{nm}$ is the damping rate (homogeneous line half-width) of the n -to- m molecular transition, and the energy difference between two molecular states is $\epsilon_{nm} = \epsilon_n - \epsilon_m$. The population decay rate of the intermediate state(s) $|e\rangle$ (or $|e'\rangle$) is $\tilde{\gamma}_{ee} = \tilde{\gamma}_{e'e'} = \Gamma$. Interstate dipole matrix elements are denoted μ_{kk} .

It is remarkable that for light from a stationary PDC source, each optical-field correlation function appearing in eq 7 factors into a product of two functions. We note that this expression contains the isolated-pulse nature of the laser-pulse case, in addition to the possibility of strong frequency anticorrelations,

as in the stochastic ‘classical’ field case.³³ This feature was discussed in section IV above.

It is important to compare the above behavior to that in two ‘classical’ light cases: ultrashort laser pulses, and stationary broadband (thermal-like) light. Generally, the four-time correlation functions that appear in eq 7 are given by

$$C(t_a, t_b, t_c, t_d) = \langle vac | \hat{E}^{(+)}(t_a) \hat{E}^{(+)}(t_b) \hat{\rho}_F \hat{E}^{(-)}(t_c) \hat{E}^{(-)}(t_d) | vac \rangle \quad (9)$$

where $\hat{\rho}_F$ is the density operator describing the state of the field, quantum or classical. For the case of short, coherent laser pulses, this takes the form of a product of four functions:

$$C_{\text{LASER}}(t_a, t_b, t_c, t_d) = E(t_a)E(t_b)E^*(t_c)E^*(t_d) \quad (10)$$

For the case of stationary stochastic ‘classical’ light, this becomes an ensemble average of correlated random processes,

$$C_{\text{STOCHASTIC}}(t_a, t_b, t_c, t_d) = \langle E(t_a)E(t_b)E^*(t_c)E^*(t_d) \rangle \quad (11)$$

For the photon-pair state from a PDC source, the correlation function is

$$C_{\text{PHOTONPAIR}}(t_a, t_b, t_c, t_d) = \langle vac | \hat{E}^{(+)}(t_a) \hat{E}^{(+)}(t_b) |\Psi\rangle_F \cdot_F \langle \Psi | \hat{E}^{(-)}(t_c) \hat{E}^{(-)}(t_d) | vac \rangle \quad (12)$$

For experiments in which exactly two photons are absorbed from the field, the way in which the 2D spectroscopy reveals information about the molecule is fully encoded in the form of the four-time correlation function. The three cases summarized are very different in their dependence on the four times. In the case of a laser, all four field-molecule interaction times are independently selected by experimentally controlled time delays. For the case of stationary stochastic ‘classical’ light, all four interaction times are random but interdependent. The case of the photon-pair state from a PDC source is intermediate between those two; the correlation function factors into a product of two two-time correlation functions, each representing the tight temporal correlation of photons emitted as pairs from the source, while allowing complete freedom in the times at which such pairs are created. This behavior profoundly impacts the properties of 2D optical spectroscopy, as noted in other contexts.^{21,22}

In order to evaluate eq 7 for the PDC source, we must account for the fact that each of the electric field operators is a sum of four operators: two from each of the A and B beams representing delayed (‘long’) and nondelayed (‘short’) paths through the Franson interferometer arms. This leads to 192 terms (plus their complex conjugates), which are summed together to form the excited-state population. Fortunately, the number of terms contributing to the detected signal can be greatly reduced by implementing a phase-sensitive detection scheme, as routinely performed in ‘classical’ 2DFS experiments.^{14–17} In this procedure, the phases of the fields passing through the two interferometer arms are continuously swept using acousto-optic Bragg cells, and the fluorescence is phase-synchronously detected. In this way, terms that oscillate with a specified ‘phase signature’ are isolated from all other ‘background’ signals. Recall that in the Franson interferometer, the phase signatures $\cos(\varphi_a - \varphi_b)$ and $\cos(\varphi_a + \varphi_b)$ act as identifiers for field frequency correlation and anticorrelation. Here we are interested in frequency anticorrelation, which enables us to resonantly excite a two-photon transition. We are

therefore concerned only with the ‘sum-phase’ $\exp[\pm i(\varphi_a + \varphi_b)]$ terms. In the limit of large optical bandwidth of the two-photon excitation field (and therefore short correlation time, on the order of tens of fs), only six of the 192 terms have the ‘sum-phase’ signature. We denote these surviving terms $R_{\text{DQC}(\pm)}^{e,e'}$, $R_{\text{RP}(\pm)}^{e,e'}$, and $R_{\text{NRP}(\pm)}^{e,e'}$.

Each of the six terms is given by a 3-fold time integral, which in the limit of wide-band fields, may be well approximated using two delta functions representing the tight temporal correlation of the photon-pairs emitted from the source at either the ‘early’ or the ‘late’ time. For purposes of interpretation, it is useful to express these integrals in terms of the integration time variables $t_{43} = t_4 - t_3$; $t_{32} = t_3 - t_2$; $t_{21} = t_2 - t_1$. Then

$$\begin{aligned} R_{\text{DQC}(+)}^{e,e'} &= e^{i(\varphi_a + \varphi_b)} e^{i\omega_p(T_{\text{ex}} + t_{\text{ex}})} \\ &\int_0^\infty dt_{43} e^{-(\gamma_{fe} + i\omega_p)t_{43}} \cdot \delta(t_{43} - t_{\text{ex}}) \cdot \\ &\int_0^\infty dt_{32} e^{-(\gamma_{fg} + i\omega_p)t_{32}} \cdot \int_0^\infty dt_{21} e^{-\gamma_{eg}t_{21}} \\ &\cdot \delta(t_{21} - t_{\text{ex}}) \\ R_{\text{DQC}(-)}^{e,e'} &= e^{-i(\varphi_a + \varphi_b)} e^{-i\omega_p(T_{\text{ex}} + t_{\text{ex}})} \\ &\int_0^\infty dt_{43} e^{-(\gamma_{fe} + i\omega_p)t_{43}} \cdot \delta(t_{43} - \tau_{\text{ex}}) \cdot \\ &\int_0^\infty dt_{32} e^{-(\gamma_{fg} + i\omega_p)t_{32}} \cdot \int_0^\infty dt_{21} e^{-\gamma_{eg}t_{21}} \\ &\cdot \delta(t_{21} - \tau_{\text{ex}}) \\ R_{\text{RP}(+)}^{e,e'} &= e^{i(\varphi_a + \varphi_b)} e^{i\omega_p(T_{\text{ex}} + t_{\text{ex}})} \int_0^\infty dt_{43} e^{-(\gamma_{fe}^* - i\omega_p)t_{43}} \\ &\int_0^\infty dt_{32} e^{-\gamma_{ee}t_{32}} \cdot \delta(t_{32} - t_{\text{ex}}) \int_0^\infty dt_{21} e^{-\gamma_{eg}t_{21}} \\ &\cdot \delta(t_{43} + t_{32} + t_{21} - \tau_{\text{ex}}) \\ R_{\text{RP}(-)}^{e,e'} &= e^{-i(\varphi_a + \varphi_b)} e^{-i\omega_p(T_{\text{ex}} + t_{\text{ex}})} \\ &\int_0^\infty dt_{43} e^{-(\gamma_{fe}^* - i\omega_p)t_{43}} \int_0^\infty dt_{32} e^{-\gamma_{ee}t_{32}} \\ &\cdot \delta(t_{32} - \tau_{\text{ex}}) \int_0^\infty dt_{21} e^{-\gamma_{eg}t_{21}} \\ &\cdot \delta(t_{43} + t_{32} + t_{21} - \tau_{\text{ex}}) \\ R_{\text{NRP}(+)}^{e,e'} &= e^{i(\varphi_a + \varphi_b)} e^{i\omega_p(T_{\text{ex}} + t_{\text{ex}})} \\ &\int_0^\infty dt_{43} e^{-(\gamma_{fe} + i\omega_p)t_{43}} \int_0^\infty dt_{32} e^{-\gamma_{ee}t_{32}} \\ &\int_0^\infty dt_{21} e^{-\gamma_{eg}t_{21}} \cdot \delta(t_{32} + t_{21} - \tau_{\text{ex}}) \\ &\cdot \delta(t_{43} + t_{32} - \tau_{\text{ex}}) \\ R_{\text{NRP}(-)}^{e,e'} &= e^{-i(\varphi_a + \varphi_b)} e^{-i\omega_p(T_{\text{ex}} + t_{\text{ex}})} \\ &\int_0^\infty dt_{43} e^{-(\gamma_{fe} + i\omega_p)t_{43}} \int_0^\infty dt_{32} e^{-\gamma_{ee}t_{32}} \\ &\int_0^\infty dt_{21} e^{-\gamma_{eg}t_{21}} \cdot \delta(t_{32} + t_{21} - \tau_{\text{ex}}) \\ &\cdot \delta(t_{43} + t_{32} - \tau_{\text{ex}}) \end{aligned} \quad (13)$$

Explicit results for each of these integrals are given in the SI. Here we focus on understanding the physical meaning of each.

The integrals in eq 13 are different from those resulting from exciting the molecule with ‘classical’ (coherent-state) ultrashort laser pulses. In the classical case (in the semi-impulsive limit), each interaction occurs at a specified, predetermined time, which is defined by the arrival of each laser pulse. In contrast,

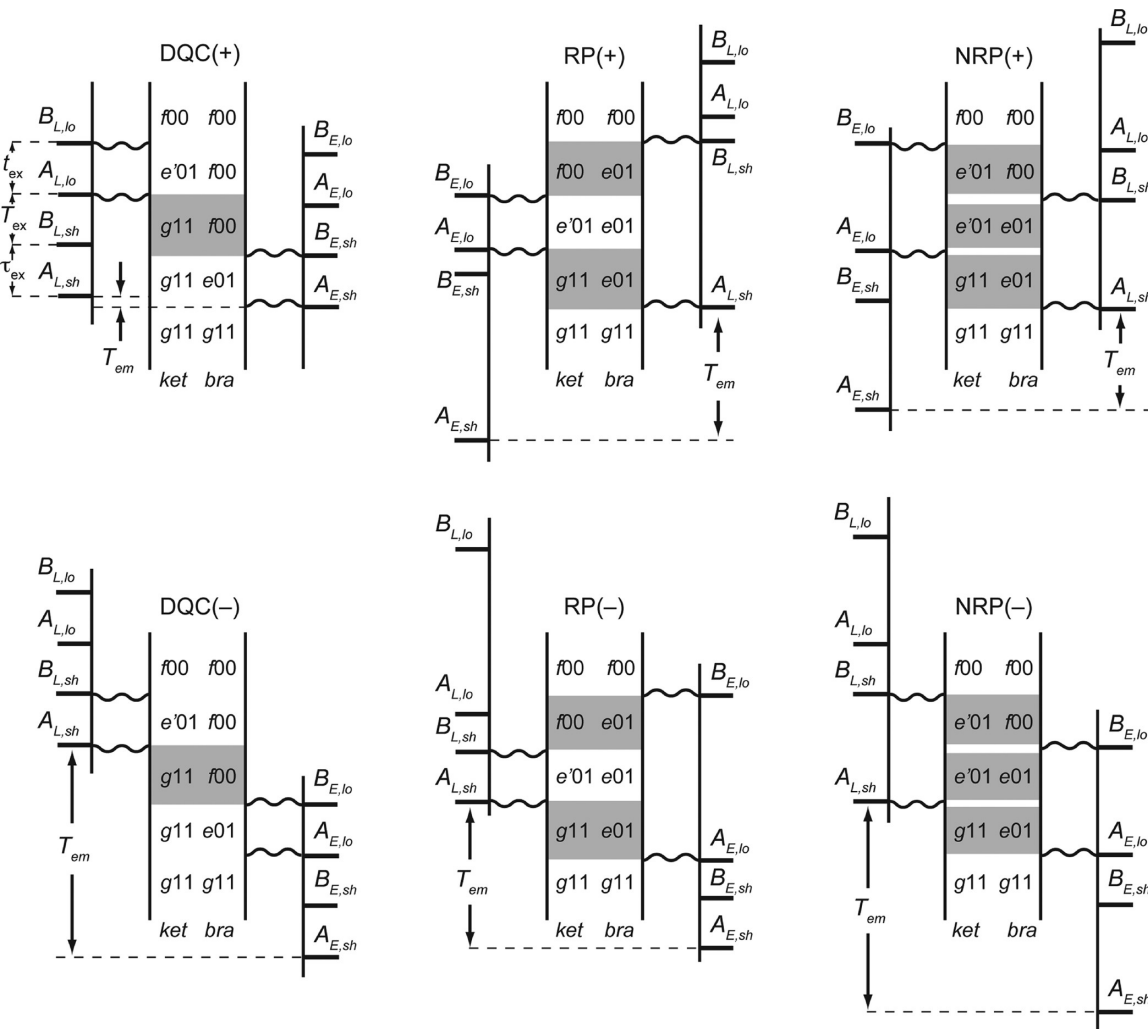


Figure 5. Double-sided Feynman diagrams for the composite field-molecule system, labeled $DQC(\pm)$, $RP(\pm)$, and $NRP(\pm)$, represent the six nonzero integrals [eq 13] with the corresponding phase signatures $\exp[\pm i(\varphi_a + \varphi_b)]$. Each excitation pathway for the classical field – molecule system (previously shown in Figure 3) gives rise to two distinct field-molecule pathways for the composite system, which include information about the quantum numbers of the exciting fields. Pathways for ‘early’ (E) and ‘late’ (L) virtual emission events are shown, and the times of their field-molecule interactions are indicated by wavy horizontal lines. The shaded regions are those with indeterminate durations between any pair of ‘early’ and ‘late’ virtual emission events, which are integrated over specific limits for each term. For example, the $DQC(\pm)$ term represents an integral in which the first two interactions are from a virtual emission event at the early time, and whose wave packets follow ‘short’ (sh) arms in their respective interferometers, while the third and fourth interactions are from a source virtual emission event at a later time, and whose wave packets follow ‘long’ (lo) arms in their interferometers.

the integrals for the entangled-photon-pair excitation involve interactions that occur over a range of unspecified times, and which must be averaged over as a consequence of the emission-time freedom. The effect is similar to the one discussed above in connection with the Franson interferometer. To clarify this point, we reformulate each integral in eq 13 in terms of the source emission-time delay, denoted by T_{em} , which is the time between the ‘early’ and ‘late’ occurrences of the photon-pair virtual emissions in the source. For each diagram, T_{em} has a unique relation to the interaction times, and takes on a different range of values.

For example, in the $R_{DQC(+)}^{e'e'}$ term, we have the two relations enforced by the delta functions: $t_{21} = \tau_{ex}$ and $t_{43} = t_{ex}$. In this case, it is useful to make the change of variables from t_{32} to the emission-time delay T_{em} , where $T_{em} = t_{32} - T_{ex}$. The integral can then be written

$$R_{DQC(+)}^{e'e'} = e^{i(\varphi_a + \varphi_b)} e^{i\omega_p T_{ex}} \int_{-T_{ex}}^{\infty} dT_{em} e^{-\gamma_{eg} \tau_{ex}} e^{-(\gamma_{fg} + i\omega_p) t_{32}^{DQC(+)}[T_{em}]} \cdot e^{-\gamma_{fg} t_{ex}} \quad (14)$$

where we introduced the function $t_{32}^{DQC(+)}[T_{em}] \equiv T_{em} + T_{ex}$, which is the delay between interactions 2 and 3 in the ‘molecular-perspective.’ The integral in eq 14 serves to sum over the many possible durations of this interval, in contrast to the classical case.

To interpret eq 14 for this integral for the DQC process, we recall that $\gamma_{nm} = \tilde{\gamma}_{nm} - i\omega_{nm}$, where $\tilde{\gamma}_{eg}$ is the damping rate (homogeneous line half-width) of the n -to- m molecular transition, and $\omega_{nm} = (\epsilon_n - \epsilon_m)/\hbar$. Reading the terms inside the integrand from left to right: at time 0, the first A interaction creates the $g-e$ coherence, which damps at a rate $\tilde{\gamma}_{eg}$ for the duration τ_{ex} , at which time the first B interaction creates the $f-g$ coherence. The $f-g$ coherence oscillates and decays at a rate $\tilde{\gamma}_{fg}$ for an indeterminate duration $t_{32}^{DQC(+)}[T_{em}]$ before the next A

interaction occurs, creating the $f-e$ coherence. This damps for a duration t_{ex} at which time the final B interaction creates population in the $|f\rangle$ state. The emission-time freedom allows the two virtual source-emission events to be separated by an interval with values in the range $[-T_{ex}, \infty]$, and the integration of eq 14 sums over this time range.

It is perhaps surprising that the result in eq 14 does not explicitly dampen during the middle experimental interval T_{ex} but oscillates instead. We note that all six terms given by eq 13 depend on T_{ex} in this manner. In eq 14, the $\tilde{\gamma}_{fg}$ damping rate, which might be expected to act during the middle interval, acts over the potentially infinite duration of the T_{em} integral, leading to a Lorentzian line shape factor, as given below.

$R_{DQC(+)}^{e,e'}$ can be represented uniquely by a double-sided Feynman diagram, labeled $DQC(+)$ in Figure 5. Here we have modified the standard diagrams to emphasize several points: (1) each ket represents the state of the composite molecule-field system: $|i, n_A, n_B\rangle$ means the molecule is in state i , where $i \in \{g, e, e', f\}$, the A field contains n_A photons, and the B field contains n_B photons. Each bra $\langle i', n_A', n_B'|$ has a similar meaning. (2) The extra time axes on both sides of the ket–bra axes indicate the virtual source emission events that contribute to a given diagram. (3) The delay T_{em} between ‘early’ and ‘late’ virtual emission events in the source is indicated in each diagram, allowing the left source axis to ‘slide,’ within limits, relative to the right source axis. This reflects the fact that the four-time correlation function in each integral in eq 7 factors into the product of two separate correlation functions. (4) The shaded gray regions indicate intervals whose durations are not fixed by the experimental delay parameters, and which must be integrated over. For the case of the $R_{DQC(+)}^{e,e'}$ term, the shaded gray region represents the $t_{32}^{DQC(+)}[T_{em}]$ interval.

In our proposed experiment, the middle delay T_{ex} is set to a fixed value while the other two delays, τ_{ex} and t_{ex} are scanned to acquire data that can be numerically Fourier Transformed with respect to these control variables. This creates the 2DFS spectrum, which includes contributions from all six terms listed above. For example, the contribution to the spectrum from the

term $R_{DQC(+)}^{e,e'}$ is

$$\begin{aligned} S_{DQC(+)}^{e,e'}(\omega_r, \omega_t) &= \sum_{e,e'} \int_0^\infty d\tau_{ex} \int_0^\infty dt_{ex} e^{-i(\omega_r \tau_{ex} + \omega_t t_{ex})} R_{DQC(+)}^{e,e'} \\ &= e^{i(\varphi_a + \varphi_b)} e^{i\omega_p T_{ex}} \sum_{e,e'} \frac{1}{\tilde{\gamma}_{fg} - i(\omega_{fg} - \omega_p)} \cdot \frac{1}{\tilde{\gamma}_{eg} - i(\omega_{eg} - \omega_r)} \\ &\quad \frac{1}{\tilde{\gamma}_{fe'} - i(\omega_{fe'} - \omega_t)} \end{aligned} \quad (15)$$

The other five integrals are evaluated similarly. In the case of the $R_{DQC(-)}^{e,e'}$ term, for example, we define a ‘molecular-perspective’ interval function $t_{32}^{DQC(-)}[T_{em}] = T_{em} - \tau_{ex} - T_{ex} - t_{ex}$. This term may then be rewritten

$$\begin{aligned} R_{DQC(-)}^{e,e'} &= e^{-i(\varphi_a + \varphi_b)} e^{-i\omega_p(T_{ex} + t_{ex})} \int_{\tau_{ex} + T_{ex} + t_{ex}}^\infty dT_{em} e^{-\tilde{\gamma}_{eg} t_{ex}} \\ &\quad e^{-(\gamma_{fg} + i\omega_p)t_{32}^{DQC(-)}[T_{em}]} e^{-(\gamma_{fe'} + i\omega_p)\tau_{ex}} \end{aligned} \quad (16)$$

This integral can be uniquely represented by the $DQC(-)$ diagram in Figure 5. Following the initial A_{Elo} interaction, in the first period of evolution, of duration t_{ex} , the $g-e$ coherence damps with rate $\tilde{\gamma}_{eg}$. During the next interval of duration $t_{32}^{DQC(-)}[T_{em}]$, indicated by the shaded region, the $g-f$ coherence

dampens with rate $\tilde{\gamma}_{fg}$. During the final interval of duration τ_{ex} the $e-f$ coherence damps with rate $\tilde{\gamma}_{fe'}$. We note that the relationship between the $DQC(-)$ and $DQC(+)$ terms is one in which the experimentally controlled intervals t_{ex} and τ_{ex} are exchanged. This symmetry is a direct consequence of the emission-time freedom.

For $R_{RP(+)}^{e,e'}$, we define two molecular-perspective times as $t_{21}^{RP(+)}[T_{em}] = T_{ex} + \tau_{ex} - T_{em}$ and $t_{43}^{RP(+)}[T_{em}] = T_{em} - T_{ex} - t_{ex}$. Then

$$\begin{aligned} R_{RP(+)}^{e,e'} &= e^{i(\varphi_a + \varphi_b)} e^{i\omega_p(T_{ex} + t_{ex})} \int_{T_{ex} + t_{ex}}^{T_{ex} + \tau_{ex}} dT_{em} e^{-\tilde{\gamma}_{eg} t_{21}^{RP(+)}[T_{em}]} \\ &\quad \cdot e^{-\Gamma t_{ex}} e^{-(\gamma_{fe'}^* - i\omega_p)t_{43}^{RP(+)}[T_{em}]} \Theta(\tau_{ex} - t_{ex}) \end{aligned} \quad (17)$$

where Θ is the Heaviside theta function. For $R_{RP(-)}^{e,e'}$, we define two molecular-perspective times as $t_{21}^{RP(-)}[T_{em}] = T_{em} - T_{ex} - \tau_{ex}$ and $t_{43}^{RP(-)}[T_{em}] = T_{ex} + t_{ex} - T_{em}$. Then

$$\begin{aligned} R_{RP(-)}^{e,e'} &= e^{-i(\varphi_a + \varphi_b)} e^{-i\omega_p(T_{ex} + t_{ex})} \int_{T_{ex} + \tau_{ex}}^{T_{ex} + t_{ex}} dT_{em} e^{-\tilde{\gamma}_{eg} t_{21}^{RP(-)}[T_{em}]} e^{-\gamma_{ee'} \tau_{ex}} \\ &\quad \cdot e^{-(\gamma_{fe'}^* - i\omega_p)t_{43}^{RP(-)}[T_{em}]} \Theta(t_{ex} - \tau_{ex}) \end{aligned} \quad (18)$$

For $R_{NRP(+)}^{e,e'}$, we define three molecular-perspective times as $t_{21}^{NRP(+)}[T_{em}] = T_{ex} + \tau_{ex} - T_{em}$, $t_{32}^{NRP(+)}[T_{em}] = T_{em} - T_{ex}$ and $t_{43}^{NRP(+)}[T_{em}] = T_{ex} + t_{ex} - T_{em}$. Then

$$\begin{aligned} R_{NRP(+)}^{e,e'} &= e^{i(\varphi_a + \varphi_b)} e^{i\omega_p(T_{ex} + t_{ex})} \int_{T_{ex}}^{T_{ex} + l(\tau_{ex}, t_{ex})} dT_{em} e^{-\tilde{\gamma}_{eg} t_{21}^{NRP(+)}[T_{em}]} \\ &\quad e^{-\gamma_{ee'} t_{32}^{NRP(+)}[T_{em}]} e^{-(\gamma_{fe'} + i\omega_p)t_{43}^{NRP(+)}[T_{em}]} \end{aligned} \quad (19)$$

where $l(x,y)$ stands for the lesser of x,y .

Finally, for $R_{NRP(-)}^{e,e'}$, we define three molecular-perspective times as $t_{21}^{NRP(-)}[T_{em}] = T_{em} - T_{ex} - \tau_{ex}$, $t_{32}^{NRP(-)}[T_{em}] = \tau_{ex} + T_{ex} + t_{ex} - T_{em}$ and $t_{43}^{NRP(-)}[T_{em}] = T_{em} - T_{ex} - t_{ex}$. Then

$$\begin{aligned} R_{NRP(-)}^{e,e'} &= e^{-i(\varphi_a + \varphi_b)} e^{-i\omega_p(T_{ex} + t_{ex})} \int_{T_{ex} + g(\tau_{ex}, t_{ex})}^{\tau_{ex} + T_{ex} + t_{ex}} dT_{em} e^{-\tilde{\gamma}_{eg} t_{21}^{NRP(-)}[T_{em}]} \\ &\quad e^{-\gamma_{ee'} t_{32}^{NRP(-)}[T_{em}]} e^{-(\gamma_{fe'} + i\omega_p)t_{43}^{NRP(-)}[T_{em}]} \end{aligned} \quad (20)$$

where $g(x,y)$ stands for the greater of x,y .

Explicit formulas for the EPP-2DFS response functions from each of these five integrals are given in the SI section.

VI. MODEL SPECTRA FOR AN ELECTRONICALLY COUPLED MOLECULAR DIMER

We now consider the EPP-2DFS observable of an electronically coupled molecular dimer. The spectroscopic properties of an electronically coupled dimer depend sensitively on the spatial relationship between the component monomer electric transition dipole moments (i.e., its ‘conformation’), in addition to the interactions between the internally coupled dimer and its local environment. Such dimers can be excellent spectroscopic probes of the local structure and dynamics of biological macromolecules, such as DNA,^{17,53–55} and phospholipid membranes.^{15,16,18,56} Moreover, electronically coupled chromophore arrays play a central role in natural photosynthetic systems,^{57,58} and they are important to developing strategies for molecular electronics technologies.⁵⁹ The electronic interactions within a coupled dimer affect linear spectroscopic signals in a variety of ways, giving rise to spectral line shifts and line shape changes, circular dichroism signals (for chiral geo-

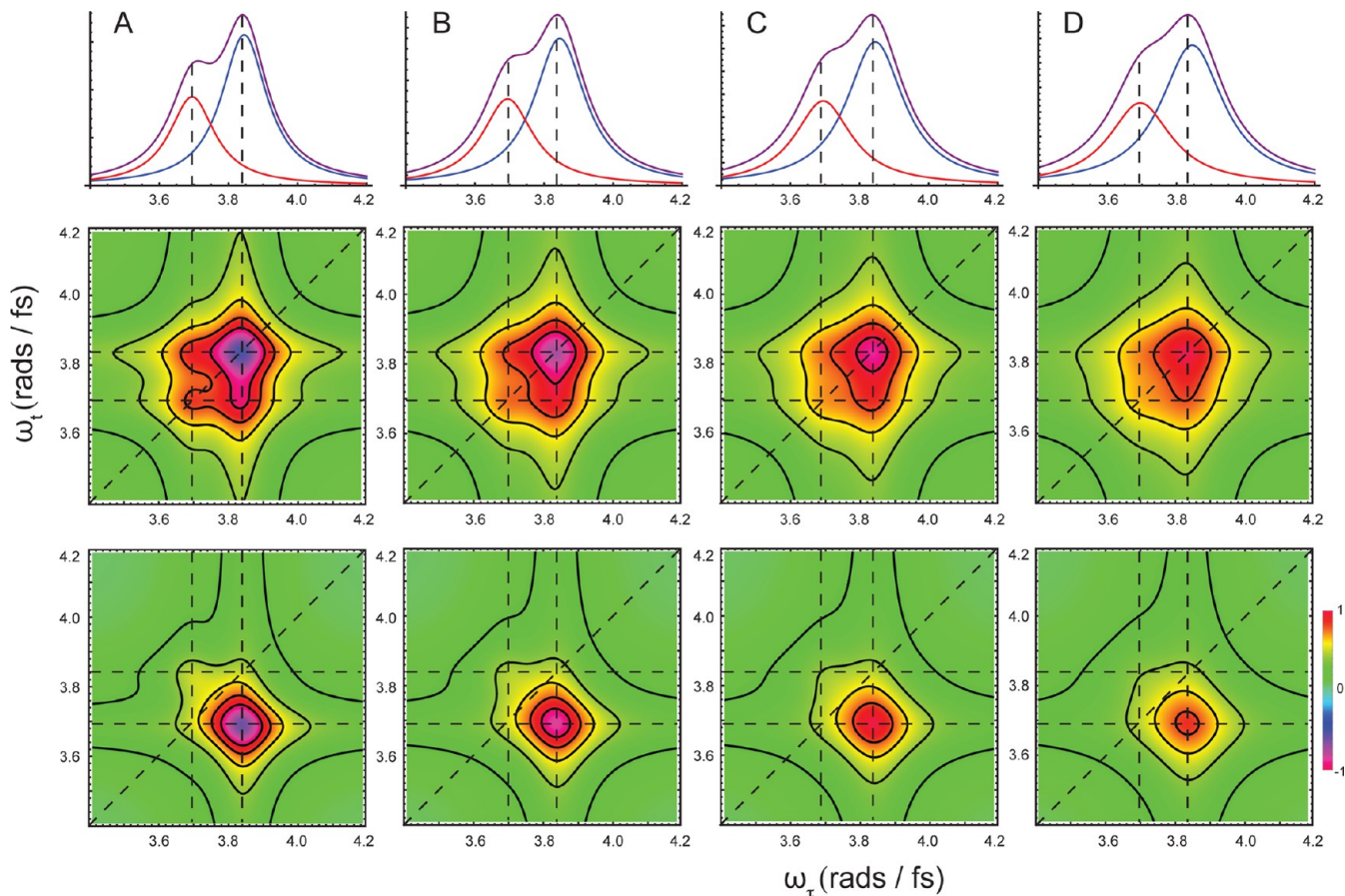


Figure 6. Simulated classical-light-excited linear and 2DFS spectra of an electronically coupled molecular dimer. The point dipole approximation was used to model a side-to-side arrangement of coupled transition dipole moments (H-dimer) with twist angle 75° , coupling strength $+400\text{ cm}^{-1}$, and monomer transition energy 3.77 rads fs^{-1} (500 nm). The $|e\rangle$ and $|e'\rangle$ state population relaxation rates have been set to $\tilde{\gamma}_{ee} = \tilde{\gamma}_{e'e'} = \Gamma = 0.03\text{ fs}^{-1}$, and the dephasing rates $\tilde{\gamma}_{ee} = 0.04\text{ fs}^{-1}$ and $\tilde{\gamma}_{fg} = 0.07\text{ fs}^{-1}$. The remaining dephasing rates $\tilde{\gamma}_{eg} = \tilde{\gamma}_{ef} = \tilde{\gamma}_{fe} = \tilde{\gamma}_{ff}$ are adjusted according to (A) 0.08 fs^{-1} , (B) 0.09 fs^{-1} , (C) 0.10 fs^{-1} , and (D) 0.11 fs^{-1} . The middle row shows the real part of standard 2DFS total correlation spectra (RP + NRP), which exhibit overlapping diagonal peaks and off-diagonal cross-peaks. The bottom row shows only the contributions to the 2DFS spectra from Feynman pathways that result in population on the $|f\rangle$ state. These terms isolate the off-diagonal cross-peaks of the 2D spectra.

metries), and variations in fluorescence quantum yields.^{16,47,54} The effects of the electronic interactions within a molecular dimer are especially apparent in its 2D optical spectrum, which can reveal the couplings between electronic transitions that are often hidden under the overlapping spectral line shapes of the linear absorption spectrum.^{15,16}

In principal, the conformation of a molecular dimer can be determined by optimizing a multiparameter model under the constraints imposed by an experimental 2D spectrum, in combination with linear absorption and/or circular dichroism spectra.^{15,16} Such a fitting procedure is feasible only if the 2D spectrum can resolve the positions and intensities of individual peaks and cross-peaks. Unfortunately, in many situations of chemical interest, 2D spectral features are too congested to extract model Hamiltonian parameters. Broadening of the optical absorption line shape occurs as a result of the combined effects of inhomogeneous site energy disorder and rapid electronic dephasing, the latter resulting from significant electronic-vibrational coupling in condensed phase molecular systems. Progress has been made toward simplifying 2D optical spectra by manipulating the polarizations of the exciting laser fields,^{60–62} and thereby reducing the signal contributions from resonant features that appear on the diagonal of the 2D spectrum. Nevertheless, this approach has the undesirable effect

of reducing the overall signal strength and, under certain polarization conditions, reducing the sensitivity of the 2D spectrum to the angle between the coupled transition dipole moments of the dimer.

As discussed above in section III, in EPP-2DFS we isolate the two-photon absorption (TPA) signal proportional to the $|f\rangle$ state population by detecting only fluorescence photoelectron counts that are coincident with the absence of photoelectron counts from the A and B beams (see Figure 2a). This is possible using time-frequency-entangled photon-pairs, because for every photon in the A beam there is guaranteed to be a correlated photon in the B beam, and vice versa. Although the quality of these measurements will depend ultimately on the photo-detector efficiency, we assume ideal detection efficiency for our current purposes. A fluorescence photon that is detected with the ‘sum-phase’ signature, and which coincides with the destruction of both photons from the transmitted A and B fields must contribute to the TPA transition. A ‘background’ signal may also occur in which two separate dimer molecules each absorb one photon from the fields. However, this ‘background’ fluorescence does not oscillate with the ‘sum-phase’ signature, and therefore it can be readily separated from the TPA signal.

In ‘classical’ 2DFS experiments performed on condensed phase molecular systems, it is not possible to isolate the TPA signal (i.e., fluorescence resulting from population on the $|f\rangle$ state) apart from the signals due to competing pathways that produce populations on the singly excited $|e\rangle$ and $|e'\rangle$ states. The ‘classical’ TPA signal is the result of three excited state absorption (ESA) pathways, which are described by the Feynman diagrams shown in Figure 3. These terms can be written¹⁶

$$\text{DQC(classical)}: \frac{e^{-T(\tilde{\gamma}_{fg} - i\omega_{fg})}}{[\tilde{\gamma}_{eg} + i(\omega_\tau - \omega_{eg})][\tilde{\gamma}_{fe'} + i(\omega_t - \omega_{fe'})]} \quad (21)$$

$$\text{RP(classical)}: \frac{e^{-T(\tilde{\gamma}_{ee'} - i\omega_{ee'})}}{[\tilde{\gamma}_{eg} + i(\omega_\tau - \omega_{eg})][\tilde{\gamma}_{fe} + i(\omega_t - \omega_{fe})]} \quad (22)$$

and

$$\text{NRP(classical)}: \frac{e^{-T(\tilde{\gamma}_{ee} - i\omega_{ee})}}{[\tilde{\gamma}_{eg} + i(\omega_\tau - \omega_{eg})][\tilde{\gamma}_{fe'} + i(\omega_t - \omega_{fe'})]} \quad (23)$$

where the frequencies ω_τ and ω_t are the Fourier transform variables of the scanned time delays τ and t , respectively. The eight remaining pathways that contribute to the classical 2DFS spectrum differ from the TPA pathways in that they absorb only a single photon from the field, although each diagram involves four field-matter interactions. These pathways are well-known, and they are referred to as ground-state bleach (GSB), stimulated emission (SE) and excited-state absorption (ESA).¹⁶ In general, a weighted sum of GSB, SE, and ESA pathways contribute to the classical 2DFS spectrum, with each term proportional to the normalized fluorescence quantum yield of its final state: 0 for the $|g\rangle$ state, 1 for the $|e\rangle$ and $|e'\rangle$ states, and ~ 0.5 for the $|f\rangle$ state.¹⁵ Here we assume the factor ~ 0.5 for the $|f\rangle$ state fluorescence quantum yield to account for the rapid deactivation and partial self-quenching of this state during the fluorescence lifetime. The GSB, SE, and ESA terms are additionally weighted according to their orientationally averaged four-point product $\langle (\mu_{ab} \cdot \mathbf{e}_1)(\mu_{cd} \cdot \mathbf{e}_2)(\mu_{jk} \cdot \mathbf{e}_3)(\mu_{lm} \cdot \mathbf{e}_4) \rangle$, which takes into account the projections of the transition dipole moments onto the polarization directions of the incident fields averaged over an isotropic distribution of dimer orientations, while keeping the relative angle between monomer transition

dipole moments fixed (see eq. S6 in the SI). We note that in our calculations, we have assumed all fields to have parallel plane polarizations.

In Figure 6, we compare simulated linear and classical 2DFS spectra for an electronically coupled molecular dimer composed of chemically identical monomeric subunits. The spectra are plotted for different values of the homogeneous line width, which has been systematically varied from $0.08\text{--}0.11\text{ fs}^{-1}$ (columns a–d). The 2D spectra are presented as contour plots versus the frequency variables ω_τ and ω_t , and for a fixed value of the waiting time interval $T = 0$. The conformation-dependent transition strengths and eigen-energies are based on the point-dipole coupling model,⁴⁷ the calculation details of which are established in ref 16. The monomer transition dipole moments are arranged side-to-side, with a relative twist angle $\theta_{sd} = 75^\circ$ and electronic coupling strength $V_{sd} = +400\text{ cm}^{-1}$ (see Figure 2b). The top row shows the linear absorption spectra predicted for the dimer. The 2DFS spectra (middle row) are composed of two resonant diagonal features [at the points $(\omega_{eg}, \omega_{eg})$ and $(\omega'_{eg}, \omega'_{eg})$] and two off-diagonal cross-peaks [at the points $(\omega_{eg}, \omega'_{eg})$ and $(\omega'_{eg}, \omega_{eg})$], with relative intensities that depend on the weights assigned to the different excitation pathways. The overlapping peaks and cross-peaks become progressively more difficult to resolve as the homogeneous line width (i.e., the electronic dephasing rate) is increased. In the bottom row, we plot the contributions to the classical 2DFS spectra that arise solely from the TPA ($|f\rangle$ state population) signal, given by eqs 21–23. In this case, the most pronounced features are the off-diagonal cross-peaks, and the diagonal peaks are greatly suppressed. Even the broadest of these spectra (panel d) still contains features that are clearly positioned off the diagonal, which allows for the magnitude of the coupling and the positions of the weaker peaks to be distinguished. Clearly, the extraction of model Hamiltonian parameters from experimental 2DFS spectra would be greatly simplified if it were possible to isolate the TPA signal from the remaining signal pathways.

The equations describing the quantum-light-excited EPP-2DFS signals obtained for an exciton-coupled dimer follow from Fourier transformation of eq S28 in the SI. Each of the resulting six terms is described by one of the double-sided Feynman diagrams shown in Figure 5, and is evaluated from the double Fourier transform of the integrals in eq 14 and eqs 16–20, giving

$$\text{DQC(+)}: \frac{e^{iT_{ex}\omega_p}}{[\tilde{\gamma}_{eg} + i(\omega_{\tau_{ex}} - \omega_{eg})][\tilde{\gamma}_{fe'} + i(\omega_{\tau_{ex}} - \omega_{fe'})][\tilde{\gamma}_{fg} + i(\omega_p - \omega_{fg})]} \quad (24)$$

$$\text{DQC(-)}: \frac{e^{-iT_{ex}\omega_p}}{\{\tilde{\gamma}_{eg} + i[\omega_{\tau_{ex}} - (\omega_p - \omega_{eg})]\}\{\tilde{\gamma}_{fe'} + i[\omega_{\tau_{ex}} - (\omega_p - \omega_{fe'})]\}[\tilde{\gamma}_{fg} - i(\omega_p - \omega_{fg})]} \quad (25)$$

$$\text{RP}(+): \frac{e^{iT_{ex}\omega_p}}{\{\tilde{\gamma}_{ee'} + i[\omega_{\tau_{ex}} + \omega_{t_{ex}} - (\omega_p + \omega_{ee'})]\}[\tilde{\gamma}_{eg} + i(\omega_{\tau_{ex}} - \omega_{eg})]\{\tilde{\gamma}_{fe} + i[\omega_{\tau_{ex}} - (\omega_p - \omega_{fe})]\}} \quad (26)$$

$$\text{RP}(-): \frac{e^{-iT_{ex}\omega_p}}{\{\tilde{\gamma}_{ee'} + i[\omega_{\tau_{ex}} + \omega_{t_{ex}} - (\omega_p - \omega_{ee'})]\}\{\tilde{\gamma}_{eg} + i[\omega_{\tau_{ex}} - (\omega_p - \omega_{eg})]\}\{\tilde{\gamma}_{fe} + i(\omega_{\tau_{ex}} - \omega_{fe})\}} \quad (27)$$

$$\text{NRP}(+): \frac{e^{iT_{ex}\omega_p}}{\{\tilde{\gamma}_{ee'} + i[\omega_{\tau_{ex}} + \omega_{t_{ex}} - (\omega_p + \omega_{ee'})]\}\{\tilde{\gamma}_{eg} + i(\omega_{\tau_{ex}} - \omega_{eg})\}\{\tilde{\gamma}_{fe'} + i(\omega_{\tau_{ex}} - \omega_{fe'})\}} \quad (28)$$

$$\text{NRP}(-): \frac{e^{-iT_{ex}\omega_p}}{\{\tilde{\gamma}_{ee'} + i[\omega_{\tau_{ex}} + \omega_{t_{ex}} - (\omega_p - \omega_{ee'})]\}\{\tilde{\gamma}_{eg} + i[\omega_{\tau_{ex}} - (\omega_p - \omega_{eg})]\}\{\tilde{\gamma}_{fe'} + i[\omega_{\tau_{ex}} - (\omega_p - \omega_{fe'})]\}} \quad (29)$$

In eqs 24–29, ω_{ij} is the transition frequency between states $|i\rangle$ and $|j\rangle$, where $i, j \in \{g, e, e', f\}$ refer to the four-level exciton-coupled dimer (see Figure 2b). $\tilde{\gamma}_{ij}$ is the rate of relaxation of the coherence $|i\rangle\langle j|$, and for the case $i = j = e = e'$, $\tilde{\gamma}_{ee} = \Gamma$ the population time of state $|e\rangle$ or $|e'\rangle$. ω_p is the frequency of the pump laser prior to down-conversion, and $\omega_{\tau_{ex}}$ and $\omega_{t_{ex}}$ are the Fourier transform variables complementary to the experimentally controlled time delays τ_{ex} and t_{ex} respectively. Similar to the classical 2DFS signal discussed above, the EPP-2DFS signal is obtained by summing each pathway over the possible intermediate states, $|e\rangle$ and $|e'\rangle$, and weighting each term by the fluorescence quantum yields and orientation factors associated with the sequence of transition dipole moments involved in that pathway.

We note that for the classical 2DFS TPA spectrum (see eqs 21–23), each resonance occurs at values of ω_τ and ω_t equal to the transition frequencies of the dimer, with line widths determined by the dephasing rates of the single-quantum coherences (e.g., $\tilde{\gamma}_{eg}$). Furthermore, each of these signal terms oscillates and rapidly dampens as the waiting time T is increased. The EPP-2DFS signals described by eqs 24–29 show additional features not present in the classical 2DFS TPA signal. The natural resonances and dephasing rates are still present; however, an additional third factor appears in the denominator of each term. The pump frequency ω_p , which has no analogue in the classical signals, is present in at least one of these factors. The DQC(+) term is identical to its classical analogue, apart from a constant factor that accounts for the TPA resonance condition $\omega_p = \omega_{fg}$. This is not the case for the RP(+) and NRP(+) terms, which contain additional factors in their respective denominators that depend on $\omega_{\tau_{ex}}$, $\omega_{t_{ex}}$, and the pump frequency ω_p . These additional factors place tighter restrictions on the line shapes of the EPP-2DFS spectra in comparison to those of classical 2DFS. The relationship between (+) and (−) terms, and the appearance of the pump frequency in eqs 24–29, are a consequence of the energy conservation condition imposed by the time-frequency

entanglement of the photons. For example, whenever a resonant transition is probed at the frequency $\omega_{\tau_{ex}} = \omega_{eg}$, there is guaranteed to be an associated transition at the frequency $\omega_{t_{ex}} = \omega_p - \omega_{eg}$.

Equations 24–29 can be interpreted in terms of the diagrams in Figure 5. Consider for example the RP(+) term described by eq 26. During the interval τ_{ex} (the delay between A_{sh} and B_{sh}), the field-molecule system undergoes four successive interactions. The molecule is initially excited into a $|g\rangle\langle el|$ coherence described by the resonance condition $\omega_{\tau_{ex}} = \omega_{eg}$ then into the $|e\rangle\langle el|$ population (or the $|e'\rangle\langle el|$ coherence for $e \neq e'$), and then into the $|f\rangle\langle el|$ coherence described by the resonance condition $\omega_{\tau_{ex}} = \omega_p - \omega_{fe}$. The interval during which the molecule is in the coherence (or population) $|e'\rangle\langle el|$ falls within both the intervals τ_{ex} and t_{ex} (i.e., the delay between A_{lo} and B_{lo}), which leads to the resonance condition $\omega_{\tau_{ex}} + \omega_{t_{ex}} = \omega_p + \omega_{ee'}$.

The resonance condition $\omega_{\tau_{ex}} + \omega_{t_{ex}} = \omega_p \pm \omega_{ee'} \simeq \omega_p$ appears in both the RP(±) and NRP(±) terms, which have the effect of maximizing the signal along the antidiagonal in the 2D spectrum, with a line width determined by $\tilde{\gamma}_{ee'}$. For cases in which $e = e'$, this is a population relaxation rate, rather than the coherence dephasing rates that would otherwise lead to broadening of the line shapes in the 2D spectra. The presence of population times within the line shape functions leads to greatly narrowed spectral features in EPP-2DFS, as illustrated in Figure 7. Although the DQC(±) signals are nearly identical to their classical analogues (not shown), the RP(±) and NRP(±) spectra are significantly narrowed in the diagonal direction. Peaks that would otherwise appear on the diagonal are greatly suppressed due to the elimination of Feynman pathways that end with population on states other than $|f\rangle$.

The suppression of diagonal peaks and the narrowing of the 2D spectral line shapes make this method especially promising for the general extraction of model Hamiltonian parameters. For the specific case of the exciton-coupled molecular dimer, the peak positions are determined primarily by the magnitude

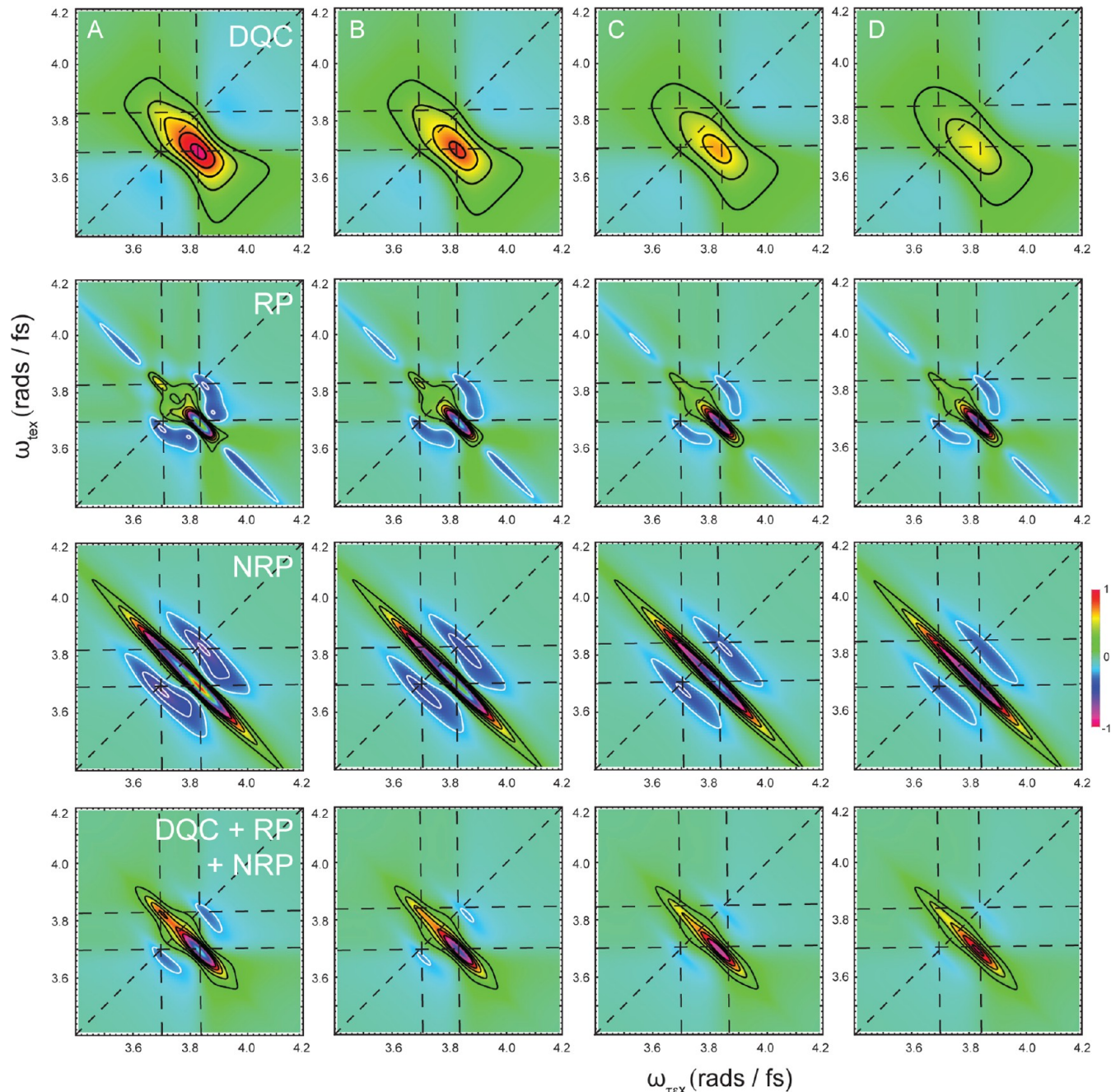


Figure 7. Simulated EPP-2DFS spectra of an electronically coupled molecular dimer using the same model parameters as for the spectra shown in Figure 6. The top row shows the DQC(\pm) terms, the second row shows the RP(\pm) terms, the third row shows the NRP(\pm) terms, and the bottom row shows the sum of all three terms. The off-diagonal cross-peaks dominate the EPP-2DFS spectra, and these features are much narrower than their classical counterparts.

of the electronic coupling, and the relative peak intensities by the angle between the monomer transition dipole moments. The EPP-2DFS method should therefore be useful for the inversion of 2D spectra to obtain the conformation of the dimer. We illustrate this point in Figure 8 by comparing the linear, ‘classical’ 2DFS, and EPP-2DFS spectra as a function of the angle between the monomer transition dipole moments θ_{sd} (see Figure 2b). As the relative dipole angle is increased from 20° – 80° , more intensity is partitioned into the otherwise weaker transition. The EPP-2DFS spectrum features a strong cross peak (below the diagonal) for all values of θ_{sd} . As θ_{sd} is

increased, the intensity of a second peak (above the diagonal) gradually increases.

In our current calculations, we did not consider the effects of inhomogeneous broadening. Our results indicate that in the homogeneous limit, EPP-2DFS presents significant advantages by narrowing 2D spectral lines and thereby reducing the effects of spectral congestion. The EPP-2DFS method may also be useful in the regime where inhomogeneous broadening becomes significant, as is often the case for complex molecular systems. While each individual photon created by the PDC source has a large uncertainty in its energy, the sum of the frequencies of the photons in any entangled pair must add to

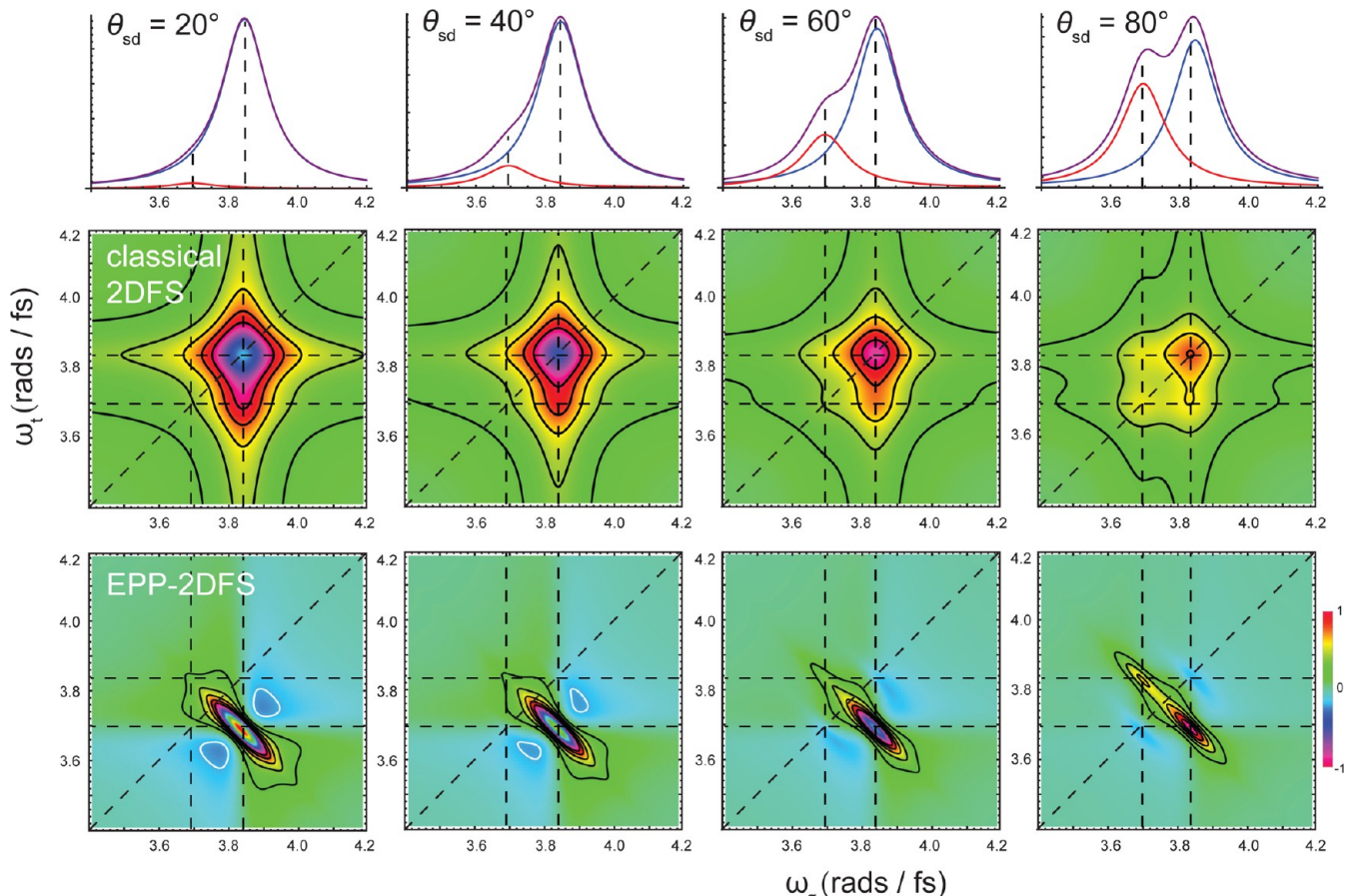


Figure 8. Simulated classical linear (top row), classical 2DFS total correlation spectra (middle row), and EPP-2DFS (bottom) for an electronically coupled molecular dimer using the same model parameters as for the spectra shown in Figures 6 and 7. The angle between the monomer transition dipole moments is varied from left to right, demonstrating the sensitivity of the EPP-2DFS observable to dimer conformation.

that of the narrow-band cw pump laser. In principle, the pump laser frequency ω_p can be tuned to a specific frequency within the inhomogeneously broadened absorption spectrum to selectively excite a small subpopulation of molecules, similar in practice to the techniques of persistent spectral hole-burning and fluorescence line narrowing.^{19,63} Only those electronically coupled dimers that match the TPA resonance condition will contribute to the signal. This apparently simultaneous high temporal and spectral resolution is possible due to the time-frequency entanglement of the photon pairs, as discussed in section IV above. The approach would allow one to selectively monitor different species in a mixture, as well as the nature of the heterogeneity that gives rise to the static site energy disorder.

VII. CONCLUSIONS

By incorporating a separated two-photon ('Franson') interferometer into the framework of a two-dimensional fluorescence spectroscopy experiment, we have proposed a new form of two-dimensional molecular spectroscopy with uniquely useful capabilities. Entangled-photon pair two-dimensional fluorescence spectroscopy (EPP-2DFS) can extract the TPA signal from electronically coupled molecular systems, while simultaneously determining the couplings between distinct electronic states. TPA processes are important to a variety of material and biological applications, such as TPA fluorescence imaging.⁶⁴ Conventional methods to measure TPA require the use of relatively high-energy ultrashort light pulses, in addition to

often-difficult experimentation to separate the weak nonlinear signal from linear 'background.' In EPP-2DFS, a cw pumped source of time-frequency-entangled photon pairs is used to excite the sample, and this leads to a number of important advantages over 'classical' ultrafast-pulse measurements. These include the enhancement of the TPA signal, which scales linearly with the excitation intensity of the entangled photons, and the suppression of the linear 'background.' Although the source is cw, the time-frequency entanglement of the photon pairs leads to the ability to probe the femtosecond Rabi oscillations associated with electronic coherences, while simultaneously selecting a narrow spectral subpopulation of molecules within an inhomogeneously broadened distribution. Finally, the 2D line shapes are greatly narrowed (with width $\sim \tilde{\gamma}_{ee}^{-1} = \tilde{\gamma}_{e'e'}^{-1} = \Gamma^{-1}$) in comparison to 'classical' 2DFS, and this too is due to the energy conservation condition imposed by the time-frequency entanglement of the field.

Test calculations performed on an electronically coupled molecular dimer suggest that the EPP-2DFS method can be useful to elucidate dimer conformation. This is because the TPA signals, which contribute only to 2D cross-peaks, can be readily separated from the one-photon absorption processes that dominate 'classical' 2DFS signals, and which contribute to 2D diagonal peaks and off-diagonal cross-peaks. We see that the greatly simplified 2D spectra are sensitive to dimer conformation. Hence, EPP-2DFS represents a promising strategy to isolate specific nonlinear signal terms, and thereby facilitate the extraction of model Hamiltonian parameters.

ASSOCIATED CONTENT

Supporting Information

Nonlinear Optical Response of an Electronically Coupled Molecular Dimer Excited by an Entangled Photon-Pair. Nonlinear Optical Response of Two Independent Molecules Excited by an Entangled Photon-Pair. This information is available free of charge via the Internet at <http://pubs.acs.org>.

AUTHOR INFORMATION

Corresponding Authors

*Phone: 541-346-4785; e-mail: raymer@uoregon.edu.

*Phone: 541-346-4809; e-mail: ahmarcus@uoregon.edu.

Author Contributions

The manuscript was written through contributions of all authors. All authors have given approval to the final version of the manuscript.

Notes

The authors declare no competing financial interest.

ACKNOWLEDGMENTS

A.H.M. would like to thank Prof. Michael D. Fayer, to whom this special issue is dedicated, for his support as a mentor and colleague over the years. This material is supported by grants from the National Science Foundation AMOP Physics and ECCS Programs (PHY-1068865 and ECCS-1101811, to M.G.R.), the NSF Chemistry of Life Processes Program (CHE-1307272, to A.H.M.), and from the Office of Naval Research (Grant N00014-11-0193, to A.H.M.). D.L.P.V. was supported by the NSF GK-12 Program (DGE-0742540). J.R.W. is a Rosaria Haugland UO Predoctoral Research Fellow.

REFERENCES

- (1) Li, Z.; Yung, M.-H.; Chen, H.; Lu, D.; Whitfield, J. D.; Peng, X.; Aspuru-Guzik, A.; Du, J. Solving quantum ground-state problems with nuclear magnetic resonance. *Sci. Rep.* **2011**, *1* (88), 1–7.
- (2) Zhu, J.; Kais, S.; Wei, Q.; Herschbach, D.; Friedrich, B. Implementation of quantum logic gates using polar molecules in pendular states. *J. Chem. Phys.* **2013**, *138*, 024104–1–7.
- (3) Mostame, S.; Rebentrost, P.; Eisfeld, A.; Kernan, A. J.; Tsomokos, D. I.; Aspuru-Guzik, A. Quantum simulator of an open quantum system using superconducting qubits: Exciton transport in photosynthetic complexes. *New J. Phys.* **2012**, *14*, 105013–1–21.
- (4) Nitzan, A. *Chemical Dynamics in Condensed Phases: Relaxation, Transfer and Reactions in Condensed Molecular Systems*; Oxford University Press: New York, 2006.
- (5) May, V.; Kühn, O., *Charge and Energy Transfer Dynamics in Molecular Systems*; Wiley-VCH: Weinheim, Germany, 2004.
- (6) Parkhill, J. A.; Tempel, D. G.; Aspuru-Guzik, A. Exciton coherence lifetimes from electronic structure. *J. Chem. Phys.* **2012**, *136*, 104510–1–9.
- (7) van Enk, S. J.; Lutkenhaus, N.; Kimble, H. J. Experimental procedures for entanglement verification. *Phys. Rev. A* **2007**, *75*, 052318–1–14.
- (8) Horodecki, R.; Horodecki, P.; Horodecki, M.; Horodecki, K. Quantum entanglement. *Rev. Mod. Phys.* **2009**, *81*, 865–942.
- (9) Chaves, R.; Davidovich, L. Robustness of entanglement as a resource. *Phys. Rev. A* **2010**, *82*, 052308–1–10.
- (10) Mandel, L.; Wolf, E. *Optical Coherence and Quantum Optics*; Cambridge University Press: Cambridge, U.K., 1995.
- (11) Franson, J. D. Bell inequalities for position and time. *Phys. Rev. Lett.* **1989**, *62*, 2205–2208.
- (12) Franson, J. D. Violations of a simple inequality for classical fields. *Phys. Rev. Lett.* **1991**, *67*, 290–293.
- (13) Franson, J. D. Two-photon interferometry over large distances. *Phys. Rev. A* **1991**, *44*, 4552–4555.
- (14) Tekavec, P. F.; Lott, G. A.; Marcus, A. H. Fluorescence-detected two-dimensional electronic coherence spectroscopy by acousto-optic phase modulation. *J. Chem. Phys.* **2007**, *127*, 214307–1–21.
- (15) Lott, G. A.; Perdomo-Ortiz, A.; Utterback, J. K.; Widom, J. R.; Aspuru-Guzik, A.; Marcus, A. H. Conformation of self-assembled porphyrin dimers in liposome vesicles by phase-modulation 2D fluorescence spectroscopy. *Proc. Natl. Acad. Sci. U.S.A.* **2011**, *108*, 16521–16526.
- (16) Perdomo-Ortiz, A.; Widom, J. R.; Lott, G. A.; Aspuru-Guzik, A.; Marcus, A. H. Conformation and Electronic Population Transfer in Membrane-Supported Self-Assembled Porphyrin Dimers by 2D Fluorescence Spectroscopy. *J. Phys. Chem. B* **2012**, *116*, 10757–10770.
- (17) Widom, J. R.; Johnson, N. P.; von Hippel, P. H.; Marcus, A. H. Solution conformation of 2-aminopurine dinucleotide determined by two-dimensional fluorescence spectroscopy. *New J. Phys.* **2013**, *15*, 025028–1–16.
- (18) Widom, J. R.; Lee, W.; Perdomo-Ortiz, A.; Rappoport, D.; Molinski, T. F.; Aspuru-Guzik, A.; Marcus, A. H. Temperature-dependent conformations of a membrane supported zinc porphyrin tweezer by 2D fluorescence spectroscopy. *J. Phys. Chem. A* **2013**, *117*, 6171–84.
- (19) Mukamel, S., *Principles of Nonlinear Optical Spectroscopy*; Oxford University Press: Oxford, 1995.
- (20) Cho, M. *Two-Dimensional Optical Spectroscopy*, 1st ed.; CRC Press: Boca Raton, FL, 2009.
- (21) Richter, M.; Mukamel, S. Ultrafast double-quantum-coherence spectroscopy of excitons with entangled photons. *Phys. Rev. A* **2010**, *82*, 013820–1–7.
- (22) Roslyak, O.; Mukamel, S. Multidimensional pump–probe spectroscopy with entangled twin-photon states. *Phys. Rev. A* **2009**, *79*, 063409–1–11.
- (23) Roslyak, O.; Marx, C. A.; Mukamel, S. Nonlinear spectroscopy with entangled photons: Manipulating quantum pathways of matter. *Phys. Rev. A* **2009**, *79*, 033832–1–5.
- (24) Gea-Banacloche, J. Two-photon absorption of nonclassical light. *Phys. Rev. Lett.* **1989**, *62*, 1603–1606.
- (25) Javanainen, J.; Gould, P. L. Linear intensity of a two-photon transition rate. *Phys. Rev. A* **1990**, *41*, 5088–5091.
- (26) Georgiades, N. P.; Polzik, E. S.; Kimble, H. J. Atoms as nonlinear mixers for detection of quantum correlations at ultrahigh frequencies. *Phys. Rev. A* **1997**, *55*, R1605–R1608.
- (27) Georgiades, N. P.; Edamatsu, K.; Kimble, H. J. Nonclassical excitation for atoms in a squeezed vacuum. *Phys. Rev. Lett.* **1995**, *75*, 3426–3429.
- (28) Lee, D.-I.; Goodson, T. Entangled photon absorption in an organic porphyrin dendrimer. *J. Phys. Chem. B* **2006**, *110*, 25582–25585.
- (29) Fei, H.-B.; Jost, B. M.; Popescu, S.; Saleh, B. E. A.; Teich, M. C. Entanglement-induced two-photon transparency. *Phys. Rev. Lett.* **1997**, *78*, 1679–1612.
- (30) Peřina, J.; Saleh, B. E. A.; Teich, M. C. Multiphoton absorption cross section and virtual-state spectroscopy for the entangled n-photon state. *Phys. Rev. A* **1998**, *57*, 3972–3986.
- (31) Salazar, L. J.; Guzmán, D. A.; Rodríguez, F. J.; Quiroga, L. Quantum-correlated two-photon transitions to excitons in semiconductor quantum wells. *Opt. Express* **2012**, *20*, 4470–4483.
- (32) Kojima, J.; Nguyen, Q.-V. Entangled biphoton virtual-state spectroscopy of the $A2\Sigma^+ - X2\Pi$ system of OH. *Chem. Phys. Lett.* **2004**, *396*, 323–328.
- (33) Dayan, B.; Pe'er, A.; Friesem, A. A.; Silberberg, Y. Two photon absorption and coherent control with broadband down-converted light. *Phys. Rev. Lett.* **2004**, *93*, 023005–1–4.
- (34) Dayan, B. Theory of two-photon interactions with broadband down-converted light and entangled photons. *Phys. Rev. A* **2007**, *76*, 043813–1–19.
- (35) Harpham, M. R.; Süzer, Ö.; Ma, C.-Q.; Bäuerle, P.; Goodson, T. Thiophene dendrimers as entangled photon sensor materials. *J. Am. Chem. Soc.* **2009**, *131*, 973–979.

- (36) Oka, H. Efficient selective two-photon excitation by tailored quantum-correlated photons. *Phys. Rev. A* **2010**, *81*, 063819-1–4.
- (37) Oka, H. Real-time analysis of two-photon excitation by correlated photons: Pulse-width dependence of excitation efficiency. *Phys. Rev. A* **2010**, *81*, 053837-1–4.
- (38) Oka, H. Selective two-photon excitation of a vibronic state by correlated photons. *J. Chem. Phys.* **2011**, *134*, 124313-1–6.
- (39) Joobeur, A.; Saleh, B. E. A.; Teich, M. C. Spatiotemporal coherence properties of entangled light beams generated by parametric down-conversion. *Phys. Rev. A* **1994**, *50*, 3349–3361.
- (40) Chiao, R., Garrison, J. *Quantum Optics*; Oxford University Press: New York, 2008.
- (41) Ou, Z. Y.; Mandel, L. Classical treatment of the Franson two-photon correlation experiment. *J. Opt. Soc. Am. B* **1990**, *7*, 2127–2131.
- (42) Rubin, M. H.; Klyshko, D. N.; Shih, Y. H.; Sergienko, A. V. Theory of two-photon entanglement in type-II optical parametric down-conversion. *Phys. Rev. A* **1994**, *50*, 5122–5133.
- (43) Kwiat, P. G.; Vareka, W. A.; Hong, C. K.; Nathel, H.; Chiao, R. Y. Correlated two-photon interference in a dual-beam Michelson interferometer. *Phys. Rev. A* **1990**, *41*, 2910–2913.
- (44) Beach, R.; Hartmann, S. R. Incoherent photon echoes. *Phys. Rev. Lett.* **1984**, *53*, 663–666.
- (45) Asaka, S.; Nakatsuka, H.; Fujiwara, M.; Matsuoka, M. Accumulated photon echoes with incoherent light in Nd³⁺-doped silicate glass. *Phys. Rev. A* **1984**, *29*, 2286–2289.
- (46) Finkelstein, V. Atomic response to optical fluctuating fields: Temporal resolution on a scale less than pulse correlation time. *Phys. Rev. A* **1991**, *43*, 4901–4912.
- (47) Kasha, M.; Rawls, H. R.; El-Bayoumi, M. A. The exciton model in molecular spectroscopy. *Pure Appl. Chem.* **1965**, *11*, 371–392.
- (48) Dai, X.; Richter, M.; Li, H.; Bristow, A. D.; Falvo, C.; Mukamel, S.; Cundiff, S. T. Two-dimensional double-quantum spectra reveal collective resonances in an atomic vapor. *Phys. Rev. Lett.* **2012**, *108*, 193201-1–4.
- (49) Muthukrishnan, A.; Agarwal, G. S.; Scully, M. O. Inducing disallowed two-atom transitions with temporally entangled photons. *Phys. Rev. Lett.* **2004**, *93*, 093002-1–4.
- (50) Zheng, Z.; Saldanha, P. L.; Leite, J. R. R.; Fabre, C. Do entangled photons induce two-photon two-atom transitions more efficiently than other states of light? arXiv:1303.5043v1 [quant-ph]: 2013; pp 1–21.
- (51) Mancini, S.; Giovannetti, V.; Vitali, D.; Tombesi, P. Entangling macroscopic oscillators exploiting radiation pressure. *Phys. Rev. Lett.* **2002**, *88*, 120401-1–4.
- (52) Khan, I. A.; Howell, J. C. Experimental demonstration of high two-photon time-energy entanglement. *Phys. Rev. A* **2006**, *73*, 031801-1–4.
- (53) Johnson, N. P.; Baase, W. A.; von Hippel, P. H. Low-energy circular dichroism of 2-aminopurine dinucleotide as a probe of local conformation of DNA and RNA. *Proc. Natl. Acad. Sci. U.S.A.* **2004**, *101*, 3426–3431.
- (54) Datta, K.; Johnson, N. P.; Villani, G.; Marcus, A. H.; von Hippel, P. H. Characterization of the 6-methyl isoxanthopterin (6-MI) base analog dimer, a spectroscopic probe for monitoring guanine base conformations at specific sites in nucleic acids. *Nucleic Acids Res.* **2012**, *40*, 1191–1202.
- (55) Widom, J. R.; Rappoport, D.; Perdomo-Ortiz, A.; Thomsen, H.; Johnson, N. P.; von Hippel, P. H.; Aspuru-Guzik, A.; Marcus, A. H. Electronic transition moments of 6-methyl isoxanthopterin - A fluorescent analogue of the nucleic acid base guanine. *Nucleic Acids Res.* **2013**, *41*, 995–1004.
- (56) Dalisay, D. S.; Quach, T.; Molinski, T. F. Liposomal circular dichroisms. Assignment of remote stereocenters in Plakinic acids K and L from a Plakortis–Xestospongia sponge association. *Org. Lett.* **2010**, *12*, 1524–1527.
- (57) Brixner, T.; Stenger, J.; Vaswani, H. M.; Cho, M.; Blankenship, R. E.; Fleming, G. R. Two-dimensional spectroscopy of electronic couplings in photosynthesis. *Nature* **2005**, *434*, 625–628.
- (58) van Amerongen, H.; Valkunas, L.; van Grondelle, R. *Photosynthetic Excitons*; World Scientific: Singapore, 2000.
- (59) Wasielewski, M. Self-Assembly Strategies for Integrating Light Harvesting and Charge Separation in Artificial Photosynthetic Systems. *Acc. Chem. Res.* **2009**, *42*, 1910–1921.
- (60) Read, E. L.; Engel, G. S.; Calhoun, T. R.; Mančal, T.; Ahn, T. K.; Blankenship, R. E.; Fleming, G. R. Cross-peak-specific two-dimensional electronic spectroscopy. *Proc. Natl. Acad. Sci. U.S.A.* **2007**, *104*, 14203–14208.
- (61) Zanni, M.; Ge, N.-H.; Kim, Y. S.; Hochstrasser, R. M. Two-dimensional IR spectroscopy can be designed to eliminate the diagonal peaks and expose only the crosspeaks needed for structure determination. *Proc. Natl. Acad. Sci. U.S.A.* **2001**, *98*, 11265–11270.
- (62) Golonska, O.; Tokmakoff, A. Polarization-selective third-order spectroscopy of coupled vibronic states. *J. Chem. Phys.* **2001**, *115*, 297–309.
- (63) Levenson, M. D.; Kano, S. S. *Introduction to Nonlinear Laser Spectroscopy*; Academic Press: London, 1988.
- (64) So, P. T. C.; Dong, C. Y.; Masters, B. R.; Berland, K. M. Two-photon excitation fluorescence microscopy. *Annu. Rev. Biomed. Eng.* **2000**, *2*, 399–429.

Supporting Information: Entangled Photon-Pair Two-Dimensional Fluorescence Spectroscopy (EPP-2DFS)

M. G. Raymer^{1,*}, Andrew H. Marcus^{2,*}, Julia R. Widom², and Dashiell L. P. Vitullo¹

1. Oregon Center for Optics and Department of Physics, University of Oregon, Eugene, OR 97403

2. Oregon Center for Optics, Institute of Molecular Biology and Department of Chemistry, University of Oregon, Eugene, OR 97403

* Corresponding authors: raymer@uoregon.edu, ahmarcus@uoregon.edu

I. Nonlinear Optical Response of an Electronically Coupled Molecular Dimer Excited by an Entangled Photon-Pair

We begin with the standard quantum formalism used to analyze most experiments in ultrafast 2D optical spectroscopy.^{1,2} The evolution of the density operator describing the entire light-molecule composite system is given by the time-ordered expansion in the Interaction Picture.

$$\hat{\rho}(t) = \sum_{n=0}^{\infty} \hat{\rho}^{(n)}(t) , \quad (\text{S1})$$

where the n -th order term is the time-ordered integral

$$\hat{\rho}^{(n)}(t) = \left(\frac{-i}{\hbar} \right)^n \int_{-\infty}^t dt_n \int_{-\infty}^{t_n} dt_{n-1} \dots \int_{-\infty}^{t_2} dt_1 \hat{U}_0(t, t_0) \cdot \left[\hat{H}_{\text{int}}(t_n), \left[\hat{H}_{\text{int}}(t_{n-1}), \dots \left[\hat{H}_{\text{int}}(t_1), \hat{\rho}_0 \right] \right] \right] \cdot \hat{U}_0^\dagger(t, t_0) , \quad (\text{S2})$$

$\hat{\rho}_0$ is the state of the combined system at $t = 0$, and $\hat{U}_0(t, t_0)$ is the time-evolution operator for the non-interacting composite system.

We consider the interaction Hamiltonian to be the electric dipole interaction, $\hat{H}_{\text{int}}(t_n) = \hat{d}(t_n) \cdot \hat{E}(t_n)$, where the dipole operator can be represented in terms of the molecular energy eigen-states $|k\rangle$ (with energies ε_k) as $\hat{d}(t) = \hbar(\hat{\mu}^{(-)}(t) + h.a.)$, with

$$\hat{\mu}^{(-)}(t) = \sum_{k>k'} \mu_{kk'} e^{i\omega_k t} |k\rangle \langle k| e^{-i\omega_{k'} t}, \quad (\text{S3})$$

and the interstate dipole matrix elements (divided by \hbar) are denoted $\mu_{kk'}$. The amplitude of the electric field is represented by the operator $\hat{E}(t) = \hat{E}^{(+)}(t) + \hat{E}^{(-)}(t)$, where the positive-frequency component of the field is

$$\hat{E}^{(+)}(t) = \int \frac{d\omega}{2\pi} h(\omega) \hat{c}(\omega) e^{-i\omega t}. \quad (\text{S4})$$

Equation (S4) is a sum of photon creation and annihilation operators that obey $[\hat{c}(\omega), \hat{c}^\dagger(\omega')] = 2\pi\delta(\omega - \omega')$ and $h(\omega) = \sqrt{\hbar\omega/V}$, where V is a quantization volume.

In quantum theory, stochastic ‘classical’ light is defined as that which can be described by a density operator that equals a statistical (classical) mixture of coherent states [man95]:³

$$\hat{\rho}_F = \sum_{\{\alpha\}} P(\{\alpha\}) |\{\alpha\}\rangle \langle \{\alpha\}|, \quad (\text{S5})$$

where $|\{\alpha\}\rangle$ is a multimode coherent state and $P(\{\alpha\})$ is the probability for a particular multimode coherent state to occur in the ensemble.

For the case of interest, the initial state described by the density operator $\hat{\rho}_0 = \hat{\rho}_M \otimes \hat{\rho}_F$ has the electronically coupled four-level dimer system (see Fig. 2b of the main text) in its ground state $\hat{\rho}_M = |g\rangle\langle g|$, and the optical field in a two-photon state $\hat{\rho}_F = |\Psi\rangle_F \cdot {}_F\langle \Psi|$, which we define below. The final state of interest is $|f\rangle|vac\rangle$ where the molecule is in its doubly-excited state $|f\rangle$, and the field is in the vacuum state $|vac\rangle$. For the two-photon absorption (2PA) process, the lowest-order contributing term is $\hat{\rho}_{ff}^{(4)}(t) = \langle f|\hat{\rho}^{(4)}(t)|f\rangle$. We assume that all of the interactions take place during the time interval $[-\tau_w, \tau_w]$. Upon making the rotating-wave approximation, where non-energy-conserving terms such as $\hat{\mu}^{(-)} \hat{E}^{(-)}$ are neglected, we obtain

$$\begin{aligned} \hat{\rho}_{ff}^{(4)} = \sum_{e,e'} & \left(\left[\mu_{eg} \mu_{fe} \mu_{ge'} \mu_{e'f} \right]_{\mathbf{e}_1 \mathbf{e}_2 \mathbf{e}_3 \mathbf{e}_4} R_{DQC}^{e,e'} + \left[\mu_{eg} \mu_{ge'} \mu_{e'f} \mu_{fe} \right]_{\mathbf{e}_1 \mathbf{e}_2 \mathbf{e}_3 \mathbf{e}_4} R_{RP}^{e,e'} \right. \\ & \left. + \left[\mu_{eg} \mu_{ge'} \mu_{fe} \mu_{e'f} \right]_{\mathbf{e}_1 \mathbf{e}_2 \mathbf{e}_3 \mathbf{e}_4} R_{NRP}^{e,e'} \right) + cc \quad , \end{aligned} \quad (\text{S6})$$

where

$$\begin{aligned} R_{DQC}^{e,e'} &= \int_{-\tau_w}^{\tau_w} dt_4 \int_{-\infty}^{t_4} dt_3 \int_{-\infty}^{t_3} dt_2 \int_{-\infty}^{t_2} dt_1 e^{-\gamma_{eg}(t_2-t_1)} e^{-\gamma_{fs}(t_3-t_2)} e^{-\gamma_{fe}(t_4-t_3)} \cdot \langle vac | \hat{E}^{(+)}(t_4) \hat{E}^{(+)}(t_3) \hat{\rho}_F \hat{E}^{(-)}(t_1) \hat{E}^{(-)}(t_2) | vac \rangle \\ R_{RP}^{e,e'} &= \int_{-\tau_w}^{\tau_w} dt_4 \int_{-\infty}^{t_4} dt_3 \int_{-\infty}^{t_3} dt_2 \int_{-\infty}^{t_2} dt_1 e^{-\gamma_{eg}(t_2-t_1)} e^{-\gamma_{ee}(t_3-t_2)} e^{-\gamma_{fe}^*(t_4-t_3)} \cdot \langle vac | \hat{E}^{(+)}(t_3) \hat{E}^{(+)}(t_2) \hat{\rho}_F \hat{E}^{(-)}(t_1) \hat{E}^{(-)}(t_4) | vac \rangle \quad , \\ R_{NRP}^{e,e'} &= \int_{-\tau_w}^{\tau_w} dt_4 \int_{-\infty}^{t_4} dt_3 \int_{-\infty}^{t_3} dt_2 \int_{-\infty}^{t_2} dt_1 e^{-\gamma_{eg}(t_2-t_1)} e^{-\gamma_{ee}(t_3-t_2)} e^{-\gamma_{fe}(t_4-t_3)} \cdot \langle vac | \hat{E}^{(+)}(t_4) \hat{E}^{(+)}(t_2) \hat{\rho}_F \hat{E}^{(-)}(t_1) \hat{E}^{(-)}(t_3) | vac \rangle \end{aligned} \quad (\text{S7})$$

In Eq. (S6), the sum is carried out over all pathways that bridge the ground and doubly-excited $|f\rangle$ state via the singly-excited $|e\rangle$ and $|e'\rangle$ states. Terms such as $\left[\mu_{eg} \mu_{fe} \mu_{ge'} \mu_{e'f} \right]_{\mathbf{e}_1 \mathbf{e}_2 \mathbf{e}_3 \mathbf{e}_4}$ denote the three-dimensional orientational average product $\langle (\mu_{eg} \cdot \mathbf{e}_1)(\mu_{fe} \cdot \mathbf{e}_2)(\mu_{ge'} \cdot \mathbf{e}_3)(\mu_{e'f} \cdot \mathbf{e}_4) \rangle$, where \mathbf{e}_i is the polarization of the i th field interaction. In Eq. (S7), we have adopted the

standard terminology,^{1,4} where DQC stands for ‘double quantum coherence,’ RP stands for ‘rephasing,’ and NRP stands for ‘nonrephasing.’ The exponential damping functions in Eq. (S7) are equal to the e, e' component of the appropriate molecular response functions

$\langle f | \hat{\mu}^{(-)}(t_a) \hat{\mu}^{(-)}(t_b) \hat{\rho}_M \hat{\mu}^{(+)}(t_c) \hat{\mu}^{(+)}(t_d) | f \rangle$, divided by $[\mu_{eg} \mu_{fe} \mu_{ge'} \mu_{e'f}]$. They are the same as those that appear in standard treatments of 2D optical spectroscopy, which use a Kubo relaxation theory for molecular dephasing

$$\begin{aligned} \langle f | \hat{\mu}^{(-)}(t_4) \hat{\mu}^{(-)}(t_3) \hat{\rho}_M \hat{\mu}^{(+)}(t_1) \hat{\mu}^{(+)}(t_2) | f \rangle^{e,e'} &= [\mu_{eg} \mu_{fe} \mu_{ge'} \mu_{e'f}] e^{-\gamma_{eg}(t_2-t_1)} e^{-\gamma_{fg}(t_3-t_2)} e^{-\gamma_{fe}(t_4-t_3)} \\ \langle f | \hat{\mu}^{(-)}(t_3) \hat{\mu}^{(-)}(t_2) \hat{\rho}_M \hat{\mu}^{(+)}(t_1) \hat{\mu}^{(+)}(t_4) | f \rangle^{e,e'} &= [\mu_{eg} \mu_{fe} \mu_{ge'} \mu_{e'f}] e^{-\gamma_{eg}(t_2-t_1)} e^{-\gamma_{ee'}(t_3-t_2)} e^{-\gamma_{fe}^*(t_4-t_3)} \\ \langle f | \hat{\mu}^{(-)}(t_4) \hat{\mu}^{(-)}(t_2) \hat{\rho}_M \hat{\mu}^{(+)}(t_1) \hat{\mu}^{(+)}(t_3) | f \rangle^{e,e'} &= [\mu_{eg} \mu_{fe} \mu_{ge'} \mu_{e'f}] e^{-\gamma_{eg}(t_2-t_1)} e^{-\gamma_{ee'}(t_3-t_2)} e^{-\gamma_{fe}(t_4-t_3)}, \end{aligned} \quad (\text{S7.1})$$

where $\gamma_{nm} = \tilde{\gamma}_{nm} - i\omega_{nm}$, $\gamma_{nm}^* = \tilde{\gamma}_{nm} + i\omega_{nm}$; $\omega_{nm} = \epsilon_{nm}/\hbar$, and $\tilde{\gamma}_{nm}$ is the damping rate (homogeneous line half-width) of the n -to- m molecular transition, and the energy difference between two molecular states is $\epsilon_{nm} = \epsilon_n - \epsilon_m$. The population decay rate of the intermediate state(s) $|e\rangle$ (or $|e'\rangle$) is $\tilde{\gamma}_{ee} = \tilde{\gamma}_{e'e'} = \Gamma$. Interstate dipole matrix elements are denoted $\mu_{kk'}$.

We note that the required time ordering of the integrals in Eq. (S6), $t_1 < t_2 < t_3 < t_4$, cannot be violated by changing the order of the interferometer delays in the laboratory. Furthermore, if the two molecular transitions are not equal in energy, then the A and B fields could be tuned to these resonances, and the A field chosen to excite the $|e\rangle \leftarrow |g\rangle$ transition, and B the $|f\rangle \leftarrow |e\rangle$ transition.

The state of the driving field is reflected in the form of the four-time correlation function

$$C(t_a, t_b, t_c, t_d) = \langle vac | \hat{E}^{(+)}(t_a) \hat{E}^{(+)}(t_b) \hat{\rho}_F \hat{E}^{(-)}(t_c) \hat{E}^{(-)}(t_d) | vac \rangle. \quad (\text{S8})$$

For the photon-pair state from a PDC source, the field is described by a pure state given by^{5,6}

$$|\Psi\rangle_F = \sqrt{1-\xi^2} |vac\rangle + \xi \int \frac{d\omega_1}{2\pi} \int \frac{d\omega_2}{2\pi} \psi(\omega_1, \omega_2) \hat{a}^\dagger(\omega_1) \hat{b}^\dagger(\omega_2) |vac\rangle + O(\xi^2), \quad (\text{S9})$$

which is normalized according to

$$\int \frac{d\omega_1}{2\pi} \int \frac{d\omega_2}{2\pi} |\psi(\omega_1, \omega_2)|^2 = 1. \quad (\text{S10})$$

In Eq. (S10), $\zeta^2 \ll 1$ is the probability that a photon pair is present in some fictional quantization length denoted L . For a pulsed pump, L is taken large enough to encompass each pulse. Photon creation operators for beams A and B are denoted by $\hat{a}^\dagger(\omega)$ and $\hat{b}^\dagger(\omega)$, respectively.

For a PDC source that is pumped by a cw monochromatic field of frequency ω_p , we have $\psi(\omega_1, \omega_2) = \sqrt{2\pi c/L} \Psi(\omega_1) 2\pi \delta(\omega_1 + \omega_2 - \omega_p)$, and the quantum entangled photon-pair state is

$$|\Psi_{\omega_p}\rangle = \sqrt{1-\xi^2} |vac\rangle + \xi \sqrt{\frac{2\pi c}{L}} \int \frac{d\omega_1}{2\pi} \Psi(\omega_1) \hat{a}^\dagger(\omega_1) \hat{b}^\dagger(\omega_p - \omega_1) |vac\rangle. \quad (\text{S11})$$

The pure state described by Eq. (S11) is remarkable for the following reasons. It exhibits random fluctuations in the field amplitude and phase, while preserving near-perfect frequency anti-correlations between the field fluctuations. The spectral entanglement is manifest in the frequency anti-correlation of the creation operators for the A field and the B field, $\hat{a}^\dagger(\omega_1)$, and $\hat{b}^\dagger(\omega_0 - \omega_1)$, where ω_0 is the sum frequency equal to the cw pump laser frequency in the PDC source. The normalized spectrum of the A field equals $|\Psi(\omega_1)|^2$, and the B -field spectrum is

given by the same function symmetrically reflected around one-half of the pump frequency. The two-photon part of the state is non-normalizable because we are treating a stationary field. Note that the inner product of the photon-pair state defined by sum frequency ω_p with a state having a different sum frequency ω'_p is proportional to a delta function $\delta(\omega_p - \omega'_p)$. Eq. (S11) is the state that was used to calculate the coincidence counting probabilities for the Franson interferometer described in Sec. II.B of the main text.

For the photon-pair state, this leads to the correlation function

$$C_{\text{PHOTON PAIR}}(t_a, t_b, t_c, t_d) = \Phi_E(t_a, t_b) \cdot \Phi_E^*(t_d, t_c), \quad (\text{S12})$$

where $\Phi_E(t_a, t_b) = \langle \text{vac} | \hat{E}^{(+)}(t_a) \hat{E}^{(+)}(t_b) | \Psi_{\omega_0} \rangle$ can be interpreted as a two-photon wave function,⁷ which we evaluate below. Its square $|\Phi(t_a, t_b)|^2$ is the joint probability that a photon would be detected at time t_a , and that another would be detected at time t_b .

The field impinging on the coupled molecular dimer is the sum of the A and B fields. Assuming that the fields are not too broad-band, with average frequency $\bar{\omega}_{AB}$, they can then be written as $\hat{E}^{(+)}(t) \approx h_{AB} \hat{F}^{(+)}$, where $h_{AB} = \sqrt{\hbar \bar{\omega}_{AB} / V}$, and the ‘photon-flux-amplitude’ operator is

$$\hat{F}^{(+)}(t) = \hat{A}^{(+)}(t) + \hat{B}^{(+)}(t), \quad (\text{S13})$$

with bosonic field-amplitude operators for each beam

$$\hat{A}(t) = \int \frac{d\omega}{2\pi} \hat{a}(\omega) e^{-i\omega t}; \quad \hat{B}(t) = \int \frac{d\omega}{2\pi} \hat{b}(\omega) e^{-i\omega t}. \quad (\text{S14})$$

Inserting Eq. (S13) into the definition for $\Phi_E(t', t)$ gives $\Phi_E(t', t) \approx h_{AB}^2 \xi \Phi(t', t)$, where

$$\begin{aligned}\Phi(t', t) &= \xi^{-1} \langle vac | \hat{F}^{(+)}(t') \hat{F}^{(+)}(t) | \Psi \rangle_F \\ &= \xi^{-1} \langle vac | (\hat{A}^{(+)}(t') + \hat{B}^{(+)}(t')) (\hat{A}^{(+)}(t) + \hat{B}^{(+)}(t)) | \Psi \rangle_F \\ &= \xi^{-1} \langle vac | (\hat{A}(t') \hat{B}(t) + \hat{B}(t') \hat{A}(t)) | \Psi \rangle_F.\end{aligned}\quad (S15)$$

In Eq. (S15), the AA and BB self-terms are equal to zero because these correspond to annihilating two photons from the same beam, whereas each beam contains at most one photon in a given detection window. Evaluating this for the general state in Eq. (S11) leads to

$$\Phi(t', t) = \int \frac{d\omega'}{2\pi} \int \frac{d\omega}{2\pi} (\psi(\omega', \omega) + \psi(\omega, \omega')) e^{-i(\omega't' + \omega t)} \quad (S16)$$

The frequency-domain wave function appearing in Eq. (S16), $\psi(\omega', \omega) + \psi(\omega, \omega')$, can be interpreted as a wave function for a two-particle (i.e., photon) state. It automatically has the correct bosonic symmetry under particle-label exchange $\omega' \leftrightarrow \omega$.⁷ For the specific case of PDC with a monochromatic pump, Eq. (S16) gives for the two-photon wave function

$$\Phi(t', t) = \sqrt{2\pi c/L} \int \frac{d\omega}{2\pi} \Psi(\omega) \left(e^{-i(\omega t' + (\omega_p - \omega)t)} + e^{-i(\omega t + (\omega_p - \omega)t')} \right). \quad (S17)$$

Both Eqs. (S16) and (S17) are symmetric under exchange of time labels, $t \leftrightarrow t'$, which is a consequence of the bosonic nature of photons when viewed as particles. This construction allows us to switch between viewing light as comprised of quantum fields, or as quantum particles.⁷

Upon insertion of Eq. (S17) into Eq. (S6), we find that each R_X term represents a single conventional molecular perturbation diagram, and that each of these has four AB time orderings. For example, the first term is

$$R_{DQC}^{e,e'} = R_{DQC}^{e,e'}(ABAB) + R_{DQC}^{e,e'}(ABBA) + R_{DQC}^{e,e'}(BAAB) + R_{DQC}^{e,e'}(BABA) \quad (S18)$$

,

where

$$\begin{aligned} R_{DQC}^{e,e'}(ABAB) &= h_{AB}^4 \int_{-\tau_w}^{\tau_w} dt_4 \int_{-\infty}^{t_4} dt_3 \int_{-\infty}^{t_3} dt_2 \int_{-\infty}^{t_2} dt_1 e^{-\gamma_{eg}(t_2-t_1)} e^{-\gamma_{fg}(t_3-t_2)} e^{-\gamma_{fe}(t_4-t_3)} \langle vac | \hat{B}(t_4) \hat{A}(t_3) \hat{\rho}_F \hat{A}^\dagger(t_1) \hat{B}^\dagger(t_2) | vac \rangle \\ R_{DQC}^{e,e'}(ABBA) &= h_{AB}^4 \int_{-\tau_w}^{\tau_w} dt_4 \int_{-\infty}^{t_4} dt_3 \int_{-\infty}^{t_3} dt_2 \int_{-\infty}^{t_2} dt_1 e^{-\gamma_{eg}(t_2-t_1)} e^{-\gamma_{fg}(t_3-t_2)} e^{-\gamma_{fe}(t_4-t_3)} \langle vac | \hat{A}(t_4) \hat{B}(t_3) \hat{\rho}_F \hat{A}^\dagger(t_1) \hat{B}^\dagger(t_2) | vac \rangle \\ R_{DQC}^{e,e'}(BAAB) &= h_{AB}^4 \int_{-\tau_w}^{\tau_w} dt_4 \int_{-\infty}^{t_4} dt_3 \int_{-\infty}^{t_3} dt_2 \int_{-\infty}^{t_2} dt_1 e^{-\gamma_{eg}(t_2-t_1)} e^{-\gamma_{fg}(t_3-t_2)} e^{-\gamma_{fe}(t_4-t_3)} \langle vac | \hat{B}(t_4) \hat{A}(t_3) \hat{\rho}_F \hat{B}^\dagger(t_1) \hat{A}^\dagger(t_2) | vac \rangle, \\ R_{DQC}^{e,e'}(BABA) &= h_{AB}^4 \int_{-\tau_w}^{\tau_w} dt_4 \int_{-\infty}^{t_4} dt_3 \int_{-\infty}^{t_3} dt_2 \int_{-\infty}^{t_2} dt_1 e^{-\gamma_{eg}(t_2-t_1)} e^{-\gamma_{fg}(t_3-t_2)} e^{-\gamma_{fe}(t_4-t_3)} \langle vac | \hat{A}(t_4) \hat{B}(t_3) \hat{\rho}_F \hat{B}^\dagger(t_1) \hat{A}^\dagger(t_2) | vac \rangle \end{aligned} \quad (S19)$$

Given that the field density operator is $\hat{\rho}_F = |\Psi_{\omega_p}\rangle\langle\Psi_{\omega_p}|$, typical source correlation functions inside Eq. (S19) are of the form $\langle vac | \hat{B}(t_b) \hat{A}(t_a) | \Psi_{\omega_p} \rangle$ and its complex conjugate.

We next must account for the delays of the interferometers in the optical paths prior to sample incidence. As shown in Fig. 1 of the main text, the relative-arm delays for the A and B interferometers are τ_a, τ_b , respectively, and there is an additional delay T_0 introduced in the B beam. Assuming the beam splitters comprising the interferometers are 50/50 reflecting / transmitting, the A and B fields impinging on the sample are given by

$$\begin{aligned}\hat{A}(t) &= \frac{1}{2} \left(\hat{A}_0(t) + e^{i\varphi_a} \hat{A}_0(t - \tau_a) \right) \\ \hat{B}(t) &= \frac{1}{2} \left(\hat{B}_0(t - T_0) + e^{i\varphi_b} \hat{B}_0(t - \tau_b - T_0) \right),\end{aligned}\tag{S20}$$

where $\hat{A}_0(t)$ and $\hat{B}_0(t)$ are the fields emerging from the source, before the interferometer, given by Eq. (S17). The relative phases are set by the controllable phase shifts φ_a and φ_b in the A and B interferometers, respectively. Equations (S20) express that each single-photon wave packet is split into two time-separated packets, which share one photon coherently between them. Although in each event there are four packets impinging on the sample, the impinging field contains only two photons.

Upon inserting Eq. (S20) into Eq. (S19), we obtain 16 terms for each $R(WXYZ)$ term. For example,

$$\begin{aligned}R_{DQC}^{e,e'}(ABAB) &= \frac{h_{AB}^4}{16} \int_{-\tau_w}^{\tau_w} dt_4 \int_{-\infty}^{t_4} dt_3 \int_{-\infty}^{t_3} dt_2 \int_{-\infty}^{t_2} dt_1 e^{-\gamma_{eg}(t_2-t_1)} e^{-\gamma_{fg}(t_3-t_2)} e^{-\gamma_{fe}(t_4-t_3)}. \\ &\langle vac | \left(\hat{B}_0(t_4 - T_0) + e^{i\varphi_b} \hat{B}_0(t_4 - \tau_b - T_0) \right) \left(\hat{A}_0(t_3) + e^{i\varphi_a} \hat{A}_0(t_3 - \tau_a) \right) | \Psi_{\omega_p} \rangle. \\ &\langle \Psi_{\omega_p} | \left(\hat{A}_0^\dagger(t_1) + e^{-i\varphi_a} \hat{A}_0^\dagger(t_1 - \tau_a) \right) \left(\hat{B}_0^\dagger(t_2 - T_0) + e^{-i\varphi_b} \hat{B}_0^\dagger(t_2 - \tau_b - T_0) \right) | vac \rangle\end{aligned}\tag{S21}$$

From Eq. (S21), we see that there are $3 \times 4 \times 16 = 192$ terms (plus their complex conjugates) summed together to form $\hat{\rho}_{ff}^{(4)}$. The number of terms contributing to the detected signal is greatly reduced by sinusoidally modulating the two interferometer-arm phases and using a phase-sensitive scheme to detect only those terms with the same phase signature, as in ‘classical’ 2DFS.⁹ We focus only on the $\exp[\pm i(\varphi_a + \varphi_b)]$ terms, of which there are two for each of the four R_{DQC} terms. For the $R_{DQC}(ABAB)$ terms, these are

$$\begin{aligned}
R_{DQC}^{e,e'}(ABAB) = & \frac{h_{AB}^4 e^{i(\varphi_a + \varphi_b)}}{16} \int_{-\tau_w}^{\tau_w} dt_4 \int_{-\infty}^{t_4} dt_3 \int_{-\infty}^{t_3} dt_2 \int_{-\infty}^{t_2} dt_1 e^{-\gamma_{eg}(t_2-t_1)} e^{-\gamma_{fg}(t_3-t_2)} e^{-\gamma_{fe}(t_4-t_3)}. \\
& \langle vac | \hat{B}_0(t_4 - \tau_b - T_0) \hat{A}_0(t_3 - \tau_a) | \Psi_{\omega_p} \rangle \cdot \langle \Psi_{\omega_p} | \hat{A}_0^\dagger(t_1) \hat{B}_0^\dagger(t_2 - T_0) | vac \rangle \\
& + \frac{h_{AB}^4 e^{-i(\varphi_a + \varphi_b)}}{16} \int_{-\tau_w}^{\tau_w} dt_4 \int_{-\infty}^{t_4} dt_3 \int_{-\infty}^{t_3} dt_2 \int_{-\infty}^{t_2} dt_1 e^{-\gamma_{eg}(t_2-t_1)} e^{-\gamma_{fg}(t_3-t_2)} e^{-\gamma_{fe}(t_4-t_3)}. \\
& \langle vac | \hat{B}_0(t_4 - T_0) \hat{A}_0(t_3) | \Psi_{\omega_p} \rangle \cdot \langle \Psi_{\omega_p} | \hat{A}_0^\dagger(t_1 - \tau_a) \hat{B}_0^\dagger(t_2 - \tau_b - T_0) | vac \rangle.
\end{aligned} \tag{S22}$$

This reduces the number of terms to eight for each of $R_{DQC}^{e,e'}$, $R_{RP}^{e,e'}$, and $R_{NRP}^{e,e'}$. Nevertheless, for the case that the optical field is ultra-broad-band, so that it has an ultra-short coherence time, only six of these 24 terms are significant, as we show next.

To evaluate the integrals such as those in Eq. (S22), we use Eq. (S14) for the optical field state, which gives, for arbitrary times t_a, t_b ,

$$\langle vac | \hat{B}_0(t_b) \hat{A}_0(t_a) | \Psi_{\omega_p} \rangle = \xi \sqrt{\frac{2\pi c}{L}} e^{-i\omega_p t_b} \int d\omega \Psi(\omega) e^{-i\omega(t_a - t_b)}. \tag{S23}$$

Rather than choose a specific model for parametric down conversion that would predict a particular form for the spectral wave function $\Psi(\omega)$, we consider the semi-impulsive limit where the bandwidth of the light is much broader than the molecular line widths, so that the optical coherence time (and thus the photon-pair arrival-time correlation) is much shorter than the response times of the molecules. In this limit, each two-time correlation function [Eq. (S23)] becomes a delta function

$$\langle vac | \hat{B}_0(t_b) \hat{A}_0(t_a) | \Psi_{\omega_p} \rangle = \kappa \delta(t_a - t_b) e^{-i\omega_p t_b} \tag{S24}$$

for some constant κ .

Recall that we assumed a particular ordering of relative delays in the interferometer arms: $0 < T_0 < \tau_a < T_0 + \tau_b$ (the *ABAB* experimental delay order). Given this delay ordering, and using the delta-function correlation approximation [Eq. (S24)], we evaluate the integrals such as those in Eq. (S22), and find that only six are nonzero. For the *ABAB* experimental delay order, we can show that in this approximation all the $R_{DQC}^{e,e'}$ terms other than $R_{DQC}^{e,e'}(ABAB)$ are zero. Likewise, of all the $R_{RP}^{e,e'}$ and $R_{NRP}^{e,e'}$ terms, only $R_{RP}^{e,e'}(AABB)$ and $R_{NRP}^{e,e'}(AABB)$ are nonzero. These are as expected from the semi-classical theory of 2DFS. $R_{DQC}^{e,e'}(ABAB)$ represents the DQC process in which both A and B fields interact mutually to create a coherence between ground $|g\rangle$ and doubly-excited $|f\rangle$ states, then another pair of A, B interactions resolves this coherence into a population on the $|f\rangle$ state. On the other hand, the NRP and RP processes, represented by $R_{RP}^{e,e'}(AABB)$ and $R_{NRP}^{e,e'}(AABB)$, respectively, are processes in which two A interactions create a population on state $|e\rangle$ or state $|e'\rangle$, then two B interactions create population on state $|f\rangle$. We write all the nonzero terms as

$$\begin{aligned} R_{DQC}^{e,e'}(ABAB) &= \frac{\kappa^2 T_w h_{AB}^4}{16} \left(R_{DQC(+)}^{e,e'}(ABAB) + R_{DQC(-)}^{e,e'}(ABAB) \right) \\ R_{RP}^{e,e'}(AABB) &= \frac{\kappa^2 T_w h_{AB}^4}{16} \left(R_{RP(+)}^{e,e'}(AABB) + R_{RP(-)}^{e,e'}(AABB) \right) \\ R_{NRP}^{e,e'}(AABB) &= \frac{\kappa^2 T_w h_{AB}^4}{16} \left(R_{NRP(+)}^{e,e'}(AABB) + R_{NRP(-)}^{e,e'}(AABB) \right), \end{aligned} \quad (\text{S25})$$

where (+) and (-) subscripts refer to the sign of the phase signature $\exp[\pm i(\varphi_a + \varphi_b)]$. For purposes of interpretation, it is useful to express the integrals in terms of the new integration time variables

$$t_{43} = t_4 - t_3; \quad t_{32} = t_3 - t_2; \quad t_{21} = t_2 - t_1 \quad (\text{S26})$$

Under this change of variables, the six nonzero terms can be written

$$\begin{aligned}
R_{DQC(+)}^{e,e'}(ABAB) &= e^{i(\varphi_a+\varphi_b)} e^{i\omega_p \tau_b} \int_0^\infty dt_{43} e^{-(\gamma_{fe}+i\omega_p)t_{43}} \delta(t_{43} + \tau_a - \tau_b - T_0) \cdot \int_0^\infty dt_{32} e^{-(\gamma_{fg}+i\omega_p)t_{32}} \cdot \int_0^\infty dt_{21} e^{-\gamma_{eg}t_{21}} \delta(t_{21} - T_0) \\
R_{DQC(-)}^{e,e'}(ABAB) &= e^{-i(\varphi_a+\varphi_b)} e^{-i\omega_p \tau_b} \int_0^\infty dt_{43} e^{-(\gamma_{fe}+i\omega_p)t_{43}} \delta(t_{43} - T_0) \cdot \int_0^\infty dt_{32} e^{-(\gamma_{fg}+i\omega_p)t_{32}} \cdot \int_0^\infty dt_{21} e^{-\gamma_{eg}t_{21}} \delta(t_{21} + \tau_a - \tau_b - T_0) \\
R_{RP(+)}^{e,e'}(AABB) &= e^{i(\varphi_a+\varphi_b)} e^{i\omega_p \tau_b} \int_0^\infty dt_{43} e^{-(\gamma_{fe}^*+i\omega_p)t_{43}} \int_0^\infty dt_{32} e^{-\gamma_{ee'}t_{32}} \int_0^\infty dt_{21} e^{-\gamma_{eg}t_{21}} \delta(t_{32} + \tau_a - \tau_b - T_0) \delta(t_{43} + t_{32} + t_{21} - T_0) \\
R_{RP(-)}^{e,e'}(AABB) &= e^{-i(\varphi_a+\varphi_b)} e^{-i\omega_p \tau_b} \int_0^\infty dt_{43} e^{-(\gamma_{fe}^*+i\omega_p)t_{43}} \int_0^\infty dt_{32} e^{-\gamma_{ee'}t_{32}} \int_0^\infty dt_{21} e^{-\gamma_{eg}t_{21}} \delta(t_{32} - T_0) \delta(t_{43} + t_{32} + t_{21} + \tau_a - \tau_b - T_0) \\
R_{NRP(+)}^{e,e'}(AABB) &= e^{i(\varphi_a+\varphi_b)} e^{i\omega_p \tau_b} \int_0^\infty dt_{43} e^{-(\gamma_{fe}+i\omega_p)t_{43}} \int_0^\infty dt_{32} e^{-\gamma_{ee'}t_{32}} \int_0^\infty dt_{21} e^{-\gamma_{eg}t_{21}} \delta(t_{43} + t_{32} - \tau_b - T_0 + \tau_a) \delta(t_{32} + t_{21} - T_0) \\
R_{NRP(-)}^{e,e'}(AABB) &= e^{-i(\varphi_a+\varphi_b)} e^{-i\omega_p \tau_b} \int_0^\infty dt_{43} e^{-(\gamma_{fe}+i\omega_p)t_{43}} \int_0^\infty dt_{32} e^{-\gamma_{ee'}t_{32}} \int_0^\infty dt_{21} e^{-\gamma_{eg}t_{21}} \delta(t_{43} + t_{32} - T_0) \delta(t_{32} + t_{21} - \tau_b - T_0 + \tau_a)
\end{aligned} \tag{S27}$$

Upon using the relationships between the two ways of expressing the experimentally controlled intervals, $\tau_{ex} \equiv T_0$, $T_{ex} \equiv \tau_a - T_0$, and $t_{ex} \equiv T_0 + \tau_b - \tau_a$, and suppressing the labels such as $ABAB$, Eq. (S27) is written in the form Eq. (13) in the main paper.

Explicit results for each of these integrals are (suppressing $ABAB$, etc. labels):

$$\begin{aligned}
R_{DQC(+)}^{e,e'} &= \frac{e^{i(\varphi_a+\varphi_b)} e^{i\omega_p \tau_{ex}}}{\gamma_{fg} + i\omega_p} e^{-\gamma_{eg} \tau_{ex}} e^{-\gamma_{fe} t_{ex}} \\
R_{DQC(-)}^{e,e'} &= \frac{e^{-i(\varphi_a+\varphi_b)} e^{-i\omega_p \tau_{ex}}}{\gamma_{fg} + i\omega_p} e^{-(\gamma_{eg}+i\omega_p)\tau_{ex}} e^{-(\gamma_{fe}+i\omega_p)t_{ex}} \\
R_{RP(+)}^{e,e'} &= \frac{e^{i(\varphi_a+\varphi_b)} e^{i\omega_p \tau_{ex}}}{\gamma_{eg} - \gamma_{fe}^* + i\omega_p} e^{-\gamma_{ee'} t_{ex}} \left(e^{i\omega_p \tau_{ex}} e^{-\gamma_{fe}^*(\tau_{ex}-t_{ex})} - e^{i\omega_p t_{ex}} e^{-\gamma_{eg}(\tau_{ex}-t_{ex})} \right) \Theta(\tau_{ex} - t_{ex}) \\
R_{RP(-)}^{e,e'} &= \frac{e^{-i(\varphi_a+\varphi_b)} e^{-i\omega_p \tau_{ex}}}{\gamma_{eg} - \gamma_{fe}^* + i\omega_p} e^{-\gamma_{ee'} \tau_{ex}} \left(e^{-i\omega_p \tau_{ex}} e^{-\gamma_{fe}^*(t_{ex}-\tau_{ex})} - e^{-i\omega_p t_{ex}} e^{-\gamma_{eg}(t_{ex}-\tau_{ex})} \right) \Theta(t_{ex} - \tau_{ex}) \\
R_{NRP(+)}^{e,e'} &= \frac{e^{i(\varphi_a+\varphi_b)} e^{i\omega_p \tau_{ex}}}{\gamma_{eg} + \gamma_{fe}^* - \Gamma + i\omega_p} \left[\left(e^{-\gamma_{ee'} \tau_{ex}} e^{i\omega_p \tau_{ex}} e^{-\gamma_{fe}^*(t_{ex}-\tau_{ex})} - e^{-\gamma_{eg} \tau_{ex}} e^{-\gamma_{fe} t_{ex}} \right) \Theta(t_{ex} - \tau_{ex}) + \right. \\
&\quad \left. \left(e^{-\gamma_{ee'} t_{ex}} e^{i\omega_p t_{ex}} e^{-\gamma_{eg}(\tau_{ex}-t_{ex})} - e^{-\gamma_{eg} \tau_{ex}} e^{-\gamma_{fe} t_{ex}} \right) \Theta(\tau_{ex} - t_{ex}) \right] \\
R_{NRP(-)}^{e,e'} &= \frac{e^{-i(\varphi_a+\varphi_b)} e^{-i\omega_p \tau_{ex}}}{\gamma_{eg} + \gamma_{fe}^* - \Gamma + i\omega_p} \left[\left(e^{-\gamma_{ee'} \tau_{ex}} e^{-i\omega_p t_{ex}} e^{-\gamma_{eg}(t_{ex}-\tau_{ex})} - e^{-(i\omega_p + \gamma_{fe}) t_{ex}} e^{-(i\omega_p + \gamma_{fe}) \tau_{ex}} \right) \Theta(t_{ex} - \tau_{ex}) + \right. \\
&\quad \left. \left(e^{-\gamma_{ee'} t_{ex}} e^{-i\omega_p \tau_{ex}} e^{-\gamma_{fe}(\tau_{ex}-t_{ex})} - e^{-(i\omega_p + \gamma_{eg}) t_{ex}} e^{-(i\omega_p + \gamma_{fe}) \tau_{ex}} \right) \Theta(\tau_{ex} - t_{ex}) \right]
\end{aligned} \tag{S28}$$

where $\Theta(x)$ is the Heaviside theta (step) function.

The Fourier transforms of Eqs. (S28), with respect to the experimental time delays τ_{ex} and t_{ex} , provide the EPP-2DFS line shapes. These are given by Eqs. (24) – (29) in the main text.

II. Nonlinear Optical Response of Two Independent Molecules Excited by an Entangled Photon-Pair

We next consider the optical response arising when time-frequency entangled light is used to excite two independent (uncoupled) two-level molecules s and d , with single photon resonance frequencies ω_s and ω_d , respectively. Dai et al. showed that when using ‘classical’ ultrashort laser pulses to excite the system, electronic coupling in the presence of anharmonicity between pairs of two-level atoms is necessary to generate a DQC signal.¹⁰ The analogous situation in which the exciting fields are spectrally quantum entangled has been discussed by Muthukrishnan et al.,¹¹ and when using classically correlated fields by Zheng et al.¹² It is found that the mere presence of frequency anti-correlation in the A and B driving fields is sufficient to create a resonant two-photon absorption (TPA) response for the simultaneous excitation of two distant molecules when the sum of the two field frequencies $\omega_p = \omega_A + \omega_B$ is slowly swept through the sum of the two molecules’ separate resonance frequencies $\omega_0 = \omega_s + \omega_d$. This arises simply because when one field’s frequency fluctuates into resonance with one molecule, the other field automatically fluctuates into resonance with the other molecule.

Here we show that the coupled dimer response is not dependent on the frequency correlation mechanism just described, and we further consider the possible effects of such correlation. The initial state described by the density operator $\hat{\rho}_0 = \hat{\rho}_M \otimes \hat{\rho}_F$ has its ground state $\hat{\rho}_M = |g\rangle\langle g|$ and the optical field in a two-photon state $\hat{\rho}_F = |\Psi\rangle_F \cdot {}_F\langle\Psi| = |AB\rangle \cdot \langle AB|$. We consider the probability that molecule s (or molecule d) independently absorbs a photon from the A field through the transition $|e\rangle \leftarrow |g\rangle$. This is given by the second-order expression $\hat{\rho}_{ff}^{(2)}(t) = \langle f|\hat{\rho}^{(2)}(t)|f\rangle$, where the final state of interest is $|f\rangle = |e\rangle_M |B\rangle_F$. Using Eqs. (S1) – (S5) and making the rotating wave approximation, it is straightforward to show that

$$\hat{\rho}_{ff}^{(2)}(t) = \langle f | \hat{\rho}^{(2)}(t) | f \rangle = \int_{-\infty}^t dt_2 \int_{-\infty}^{t_2} dt_1 \langle f | C | f \rangle, \quad (\text{S29})$$

where

$$\begin{aligned} \langle f | C | f \rangle = & - \left\{ \langle f | \hat{\mu}_{eg}^{(-)}(t_1) \hat{E}^{(+)}(t_1) \hat{\rho}_0 \hat{\mu}_{ge}^{(+)}(t_2) \hat{E}^{(-)}(t_2) | f \rangle \right. \\ & \left. + \langle f | \hat{\mu}_{ge}^{(-)}(t_2) \hat{E}^{(+)}(t_2) \hat{\rho}_0 \hat{\mu}_{eg}^{(+)}(t_1) \hat{E}^{(-)}(t_1) | f \rangle \right\} + cc. \end{aligned} \quad (\text{S30})$$

Making use of the definitions $\hat{\mu}_{eg}^{(-)}(t_1) = \langle e | \hat{\mu}_{eg}^{(-)}(t_1) | g \rangle$, etc., we can simplify Eq. (S30)

$$\begin{aligned} \langle f | C | f \rangle = & - \left\{ \hat{\mu}_{eg}^{(-)}(t_1) \hat{\mu}_{ge}^{(+)}(t_2) \cdot \langle B | \hat{E}^{(+)}(t_1) \hat{\rho}_F \hat{E}^{(-)}(t_2) | B \rangle \right. \\ & \left. + \hat{\mu}_{eg}^{(+)}(t_1) \hat{\mu}_{ge}^{(-)}(t_2) \cdot \langle B | \hat{E}^{(+)}(t_2) \hat{\rho}_F \hat{E}^{(-)}(t_1) | B \rangle \right\} + cc. \end{aligned} \quad (\text{S31})$$

Upon substitution of the fields $\hat{E}^{(+)}(t_1) = \hat{A}(t_1) + \hat{B}(t_1)$ and $\hat{E}^{(-)}(t_1) = \hat{A}^\dagger(t_1) + \hat{B}^\dagger(t_1)$, and the expressions given by Eq. (S20) for the time-delayed A and B fields impinging on the sample, we obtain:

$$\begin{aligned} & \langle B | \hat{E}^{(+)}(t_1) \hat{\rho}_F \hat{E}^{(-)}(t_2) | B \rangle \\ &= \langle B | \hat{A}(t_1) + \hat{B}(t_1) | AB \rangle \langle AB | \hat{A}^\dagger(t_2) + \hat{B}^\dagger(t_2) | B \rangle \\ &= \langle B | \hat{A}(t_1) | AB \rangle \langle AB | \hat{A}^\dagger(t_2) | B \rangle \\ &= \langle B | \frac{1}{2} \left(\hat{A}_0(t_1) + e^{i\varphi_a} \hat{A}_0(t_1 - \tau_a) \right) | AB \rangle \langle AB | \frac{1}{2} \left(\hat{A}_0^\dagger(t_2) + e^{-i\varphi_a} \hat{A}_0^\dagger(t_2 - \tau_a) \right) | B \rangle. \end{aligned} \quad (\text{S32})$$

Equation (S32) shows that the probability that a single photon from the A beam is absorbed depends only on the phase φ_a of the A beam. A similar treatment for the absorption of a photon from the B beam leads to equivalent expressions that depend only on the phase φ_b of the B beam

$$\begin{aligned} & \langle A | \hat{E}^{(+)}(t_1) \hat{\rho}_F \hat{E}^{(-)}(t_2) | A \rangle \\ &= \langle A | \frac{1}{2} \left(\hat{B}_0(t_1) + e^{i\varphi_b} \hat{B}_0(t_1 - \tau_a) \right) | AB \rangle \langle AB | \frac{1}{2} \left(\hat{B}_0^\dagger(t_2) + e^{-i\varphi_b} \hat{B}_0^\dagger(t_2 - \tau_a) \right) | A \rangle. \end{aligned} \quad (\text{S33})$$

Regardless of any frequency correlation between the A and B fields, if only a single fluorescent photon is detected, the observed signal cannot depend on joint phase factors such as $e^{\pm(\varphi_a+\varphi_b)}$.

It is important to emphasize that for spectrally entangled light, the driving fields A and B are time-frequency entangled such that their sum frequency $\omega_p = \omega_A + \omega_B$ at all times equals $\omega_0 = \omega_s + \omega_d$, although each frequency ω_A and ω_B is fluctuating. Without frequency anti-correlation, there is no resonance when the frequencies ω_p and ω_0 are equal. However, with frequency anti-correlation there is a resonance in the TPA response that arises simply because at instants when one field is resonant with its corresponding molecule, the other field is guaranteed to also be resonant with its corresponding molecule.^{11, 12}

If we devised a way to detect the two fluorescent photons in coincidence from both molecules excited by this mechanism, then the joint probability of observing this correlated TPA process would depend on products of phase-factors, such as $e^{\pm(\varphi_a+\varphi_b)}$. Since our experimental design rests on detecting single photons (the probability to detect two photons in one detector is small), the probability of detecting one photon from each of the molecules emitted by the above mechanism is vanishingly small. Thus, the detection of a single fluorescent photon from one of the two-level molecules (regardless of whether the other molecule has been excited) would depend only on the sum of the individual one-photon absorption probabilities. Therefore, there will be no ‘background’ signal generated from separated molecules that carries the $e^{\pm(\varphi_a+\varphi_b)}$ phase signature, and our proposed scheme should not be negatively affected by this mechanism.

References

1. Mukamel, S., *Principles of Nonlinear Optical Spectroscopy*. Oxford University Press: Oxford, 1995.

2. Cho, M., *Two-Dimensional Optical Spectroscopy*. 1st ed.; CRC Press: Boca Raton, 2009.
3. Mandel, L., Emil Wolf, *Optical Coherence and Quantum Optics*. Cambridge University Press: Cambridge, 1995.
4. Perdomo-Ortiz, A., J. R. Widom, G. A. Lott, A. Aspuru-Guzik, A. H. Marcus, Conformation and Electronic Population Transfer in Membrane-Supported Self-Assembled Porphyrin Dimers by 2D Fluorescence Spectroscopy. *J. Phys. Chem. B* 2012, 116, 10757-10770.
5. Keller, T. E., M. H. Rubin, Theory of two-photon entanglement for spontaneous parametric down-conversion driven by a narrow pump pulse. *Phys. Rev. A* 1997, 56, 1534-1541.
6. Grice, W. P., A. B. U'Ren, I. A. Walmsley, Eliminating frequency and space-time correlations in multiphoton states. *Phys. Rev. A* 2001, 64, 063815-1-7.
7. Smith, B. J., M. G. Raymer, Photon wave functions, wave-packet quantization of light, and coherence theory. *New Journal of Physics* 2007, 9, 414-1-37.
8. Scully, M. O., M. S. Zubairy, *Quantum Optics*. Cambridge University Press: Cambridge, 1997.
9. Tekavec, P. F., G. A. Lott, and A. H. Marcus, Fluorescence-detected two-dimensional electronic coherence spectroscopy by acousto-optic phase modulation. *J. Chem. Phys.* 2007, 127, 214307-1-21.
10. Dai, X., M. Richter, H. Li, A. D. Bristow, C. Falvo, S. Mukamel, S. T. Cundiff, Two-dimensional double-quantum spectra reveal collective resonances in an atomic vapor. *Phys. Rev. Lett.* 2012, 108, 193201-1-4.
11. Muthukrishnan, A., G. S. Agarwal, M. O. Scully, Inducing disallowed two-atom transitions with temporally entangled photons. *Phys. Rev. Lett.* 2004, 93, 093002-1-4.
12. Zheng, Z., P. L. Saldanha, J. R. R. Leite, C. Fabre, Do entangled photons induce two-photon two-atom transitions more efficiently than other states of light? In *March 21, 2013*, Cornell University Library; arXiv:1303.5043v1 [quant-ph]: 2013; pp 1-21.